Journal of Chromatography A, 1217 (2010) 6214–6229

Contents lists available at ScienceDirect

Journal of Chromatography A

journal homepage: www.elsevier.com/locate/chroma

# Interpreting the difference between conventional and bi-directional plate-height measurements in liquid chromatography

Hui Guo, Douglas D. Frey*

*Department of Chemical and Biochemical Engineering, University of Maryland Baltimore County, 1000 Hilltop Circle, Baltimore, MD 21250, USA*

ARTICLE INFO

*Article history:*
Received 10 May 2010
Received in revised form 3 August 2010
Accepted 5 August 2010
Available online 11 August 2010

*Keywords:*
Bi-directional plate-height measurement
Theory of chromatography
Convective dispersion
*A* term
van Deemter equation

ABSTRACT

An experimental and theoretical study was conducted of the column characterization technique in which plate heights determined using the conventional pulse-response method are compared with those determined using a bi-directional method where an eluite sample is introduced into one end of a chromatographic column and elution occurs at the same end after the flow direction is reversed inside the column. Experiments are presented for a micropellicular HPLC column before and after its performance has been degraded by repeated sample injections, for a low-pressure column containing nonporous glass particles, and for an HPLC column containing particles with 300 Å pores. The results obtained are interpreted in terms of several different theories which apply in various Fourier number ranges. It was shown that the transcolumn contribution to convective dispersion in a chromatographic column is largely responsible for the difference observed between conventional and bi-directional plate-height measurements and that a collocation method can be employed to develop a useful analytical expression for this contribution.



## 1. Introduction

A large number of past studies have investigated the transport processes which determine chromatographic column performance [1–6]. The experimental and theoretical methods developed in these studies are useful for a variety of purposes, such as for the design of industrial-scale chromatographic separation processes [7], for investigating the usefulness of novel types of chromatographic packing materials [8–11], for quality control procedures when packing chromatographic columns [12,13], and for establishing the usable column lifetime as well as the success of rejuvenation protocols for fouled columns [14,15].

The simplest, and most widely used method to assess chromatographic column performance is the measurement of the theoretical plate height as a function of the mobile phase flow rate by using a pulse-response experiment in which a small feed slug containing an eluite is injected into the column entrance, and the eluite peak shape is then measured at the column exit. Results from these types of measurements are commonly fitted to equations describing mass transfer in a particulate bed, such as the van Deemter [2] or Knox equations [3–5], in order to determine pertinent fundamental physical properties for the column, such as the diffusional tortuosity inside the packing particles and the interparticle dispersion coefficient.

One characterization method that is much less widely used than the classical plate-height experiment described above is the bi-directional or reversed-flow plate-height experiment in which the flow direction is changed while the eluite of interest is inside the column. The earliest reported version of this experiment appears to be the method described by Eon [16] in which the flow direction was changed several times after the eluite was injected into column, and the eluite peak shape was then measured at the column end opposite to where the original injection was made. Somewhat later, Kaminski [17] described a related bi-directional plate-height method in which the eluite exited the same column end where the injection was made. As discussed by Kaminski, this method permits the characterization of irregularities in axial flow velocity occurring across the column radius.

More recently, Lightfoot and co-workers [18–21] applied the method of Kaminski to both process-scale particulate columns and to process-scale columns consisting of a stack of adsorptive membranes. These workers emphasized the usefulness of the method for determining how well an actual column performs in comparison to a hypothetical column containing the same packing material, but where perfect plug flow is achieved. Lightfoot and co-workers also pointed out that for the columns used in their studies where the column diameter is roughly equal to the column length, irregularities in axial flow velocity across the column radius may be caused not only by corresponding radial irregularities in the column permeability, but also by the design of the fluid headers at the column inlet and outlet. These workers also developed a modification of the original method of Kaminski which decoupled these

* Corresponding author. Tel.: +1 410 455 3418; fax: +1 410 455 6500.
*E-mail address:* dfrey1@umbc.edu (D.D. Frey).

0021-9673/$ – see front matter © 2010 Elsevier B.V. All rights reserved.
doi:10.1016/j.chroma.2010.08.010

two effects by obtaining results for presumably identically packed column of various lengths.

Despite the several studies of the bi-directional pulse-response method described above, relatively little work has been reported on the theoretical basis for interpreting these types of experiments, and especially for interpreting the differences in the results obtained for the single-directional and bi-directional pulse-response experiments. In particular, although a number of studies have investigated the effect of radial variations in axial flow velocity on eluite band shapes, these studies have been primarily numerical studies of specific, limited cases, such as the case of a parabolic velocity profile [16,22,23] and have not considered the effects of radial dispersion, which is expected to be important in many practical situations. The purpose of this study therefore is to provide convenient analytical relations based on rigorous theory that can be used by the typical practitioner of chromatography to interpret results obtained from bi-directional plate-height experiments in a wide variety of situations. In this way, it is expected that this work will facilitate the broader use of bi-directional plate-height experiments within the chromatographic community.

As mentioned above, for columns where the length is considerably larger than the column diameter, the primary effect probed by bi-directional pulse-response experiments is the variation in axial flow velocity across the column radius caused by corresponding variations in the column packing permeability. These types of experiments therefore largely measure the so-called "transcolumn" contribution to the "*A*" term of the van Deemter or Knox equations, which is the term corresponding to axial dispersion inside the column. It is therefore of interest to compare results obtained here with previous studies where direct measurements of radial variations in axial flow velocity inside chromatographic columns have been made [24–28], as well as previous studies of the relative magnitudes of the various contributions to the *A* term [4,5,29,30] and of the overall magnitude of *A* term in comparison to the other terms of the van Deemter and Knox equations [2–5].

The results of this study are expected to be of practical use for interpreting chromatographic behavior when the *A* term of the van Deemter equation yields a significant portion of the overall band broadening. This situation occurs when either nonporous particles, superficially porous (i.e., solid-core) particles, or continuous polymeric monoliths are used as column packings. In addition, this situation occurs when low-molecular-weight analytes are employed at relatively low mobile phase flow velocities for all types of column packings, or when the performance of a packed column becomes degraded through extensive use by the movement of particles from their optimal configuration inside the column. Finally, Knox has suggested that the *A* term may be significant in comparison to the other terms of the van Deemter equation under a much wider range of conditions than previously thought [4,5], in which case the results developed here may be generally useful in chromatographic studies.

## 2. Theory

### 2.1. The transcolumn contribution to convective dispersion in a cylindrical chromatographic column where the axial fluid velocity varies radially

In this section, several previous approaches for describing convective dispersion in a chromatographic column will be described and extended. In this context, the term "convective dispersion" will be used to denote the band-spreading phenomena due to the convective motion of the fluid phase in the interparticle voids. Band spreading of this type has also been termed "eddy diffusion" or "eddy dispersion" by some workers. [1,4,5]. In contrast, the band spreading which occurs in the absence of convection is presumed here to be entirely due to molecular diffusion.

As illustrated in Fig. 1, in this study the sources of convective dispersion will be subdivided into the two main categories: (1) the case where the velocity inequalities of interest vary on a length scale commensurate with the column diameter, termed here the "transcolumn" contribution to convective dispersion, and (2) the case where the velocity inequalities of interest vary on a scale significantly smaller than the column diameter, termed here the "intracolumn" contribution to convective dispersion. As also illustrated in Fig. 1, velocity inequalities at different length scales are able to exist due to the fact that the averaging volume used to determine the fluid velocity at one length scale may be larger than the length scale corresponding to the smaller velocity inequality. It will also be assumed in this section for simplicity that the particles constituting the column packing are nonporous, and that there is no adsorption of the eluite onto the particle surface, in which case all of the eluite is located in the interparticle fluid. The case of porous particles and an adsorbing eluite is considered in Appendix B.

#### 2.1.1. The close-to-equilibrium regime

Convective dispersion in an empty cylindrical tube with fully developed laminar flow and no fluid slip at walls in the "close-to-equilibrium" regime (defined as the regime where the variation in radial solute concentration is small compared to the average solute concentration) was considered first by Taylor [31,32] with later work done by Aris [33]. Subsequently, this result was extended to flow in a packed column where the radial variation in the axial flow velocity is of arbitrary shape by Giddings [1], Littlewood [6] and Bischoff and Levenspiel [34]. Of these last three studies, the simplest to apply is that of Bischoff and Levenspiel who developed an expression for the reduced axial plate height that can be written in the following form:

$$h_{CE} = \left(\frac{d_c}{d_p}\right)^2 \frac{2}{h_r} \int_0^1 \left( \int_0^\xi \left( \frac{u_f(\xi')}{u_{f,ave}} - 1 \right) \xi' \, d\xi' \right)^2 \frac{d\xi}{\xi} \tag{1}$$

In Eq. (1), $u_{f,ave}$ is the average axial interstitial fluid velocity, $u_f$ is the axial interstitial fluid velocity at a particular radial position, $h_r$ is the reduced radial plate height given by $2D_r/(u_{f,ave}d_p)$ where $D_r$ is the radial dispersion coefficient, $d_p$ is the particle diameter, and $\xi$ and $\xi'$ are dummy integration variables which represent the dimensionless column radius given by $r/R_c$ where $R_c$ is the column radius. Note that the dimensionless plate height in the close-to-equilibrium regime, $h_{CE}$, is given by $H_{CE}/d_p$, where $H_{CE}$ is the dimensional plate height.

Consider the general *n*th order velocity profile in a cylindrical column with fluid slip permitted at the column wall in the following form:

$$u_f = u_{f,cl}\left(1 - \frac{ar^n}{R_c^n}\right) \tag{2}$$

where $u_{f,cl}$ is centerline interstitial fluid velocity and *a* is fractional change in velocity across the radius. Note that when *n* is large, the majority of the fluid velocity change takes place near the column wall, which is a condition sometimes termed the "wall effect" (see Fig. 2) [35–37]. For the velocity profile given by Eq. (2), $u_f$ can be integrated across the column radius to yield the relation $u_{f,ave} = u_{f,cl}(n+2-2a)/(n+2)$. Substituting this relation into Eq. (1) and performing the indicated double integration yields:

$$h_{CE} = \frac{a^2 n^2}{2(n+2)(n+4)(2a-n-2)^2 h_r}\left(\frac{d_c}{d_p}\right)^2 \tag{3}$$

Eq. (3) is a special case of Eq. (4.5-21) of Giddings [1], which is a more general result for $h_{CE}$ for the case where $u_f$ is an arbi-

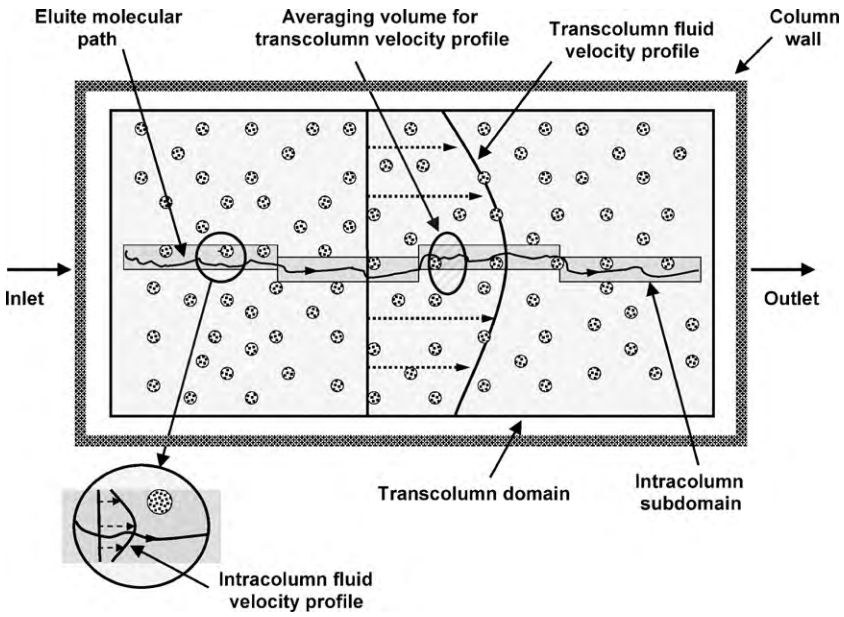


**Fig. 1.** Illustration of the transcolumn and intracolumn fluid velocity profiles inside a chromatographic column. For clarity only one category of intracolumn dispersion contribution is shown which consists of four separate subdomains.

trary power series function of $r$. When $n = 2$, Eq. (3) simplifies to the following result for a parabolic velocity profile:

$$h_{CE} = \frac{a^2}{48(2-a)^2 h_r}\left(\frac{d_c}{d_p}\right)^2 \quad (4)$$

The ability of the relations developed in this section to accurately represent experimental data depends to a large extent on the accurate representation of the plate height for radial dispersion in porous media. Numerous studies of radial dispersion [24–28] suggest that the reduced radial plate height can be expressed in terms of the reduced velocity, defined as $v = u_{f,ave} d_p / D_m$ where $D_m$ is the molecular diffusion coefficient, according to the relation $h_r = A + B/v$, where $A$ and $B$ are constant. In a randomly packed column at low flow rates, and assuming that diffusion inside the particles does not contribute to radial mass transfer inside the column, the radial dispersion coefficient becomes equal to the molecular diffusion coefficient corrected for the interparticle bed tortuosity, denoted here as $\gamma$, where the tortuosity is the inverse of the so-called obstruction factor. It then follows for this case that $D_r = D_m/\gamma$, and that at low flow velocities the radial Peclet number, defined as $Pe_r = u_{f,ave} d_p / D_r$, is given by $Pe_r = v\gamma$.

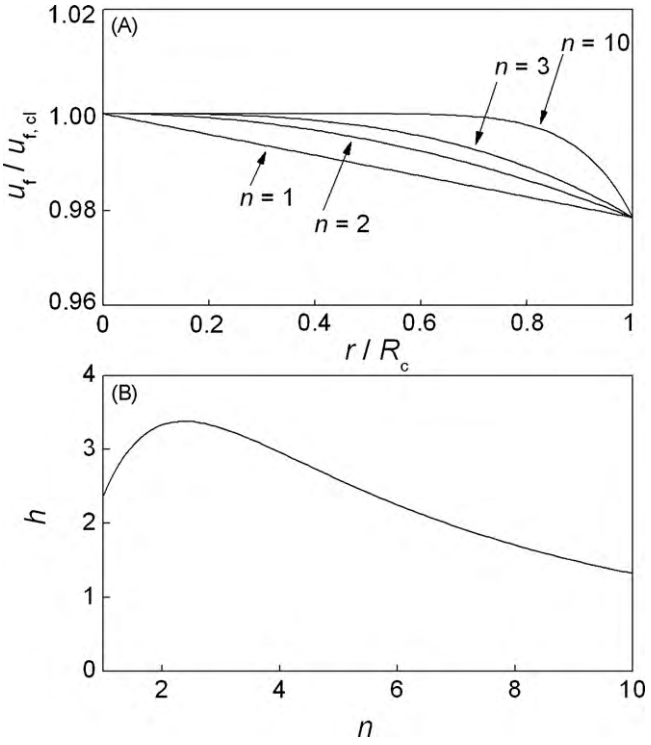


**Fig. 2.** The effect of $n$ on the fluid velocity profile and the plate height. Calculations correspond to $a = 0.02$, $d_c/d_p = 400$, and $h_r = 0.1$.

Several experimental and theoretical results for $Pe_r$ for the case of high flow velocities are summarized in Fig. 3, which shows results obtained by Tallarek et al. [25] using pulsed field gradient nuclear magnetic resonance for columns of two different particle sizes, and limiting results at high reduced velocities obtained using traditional pulse-response methods by Knox et al. [38], Eon [16], and Perkins and Johnston [39]. Note that all the results just mentioned, except the Perkins and Johnston result, were obtained using packed columns where the particle size and column dimensions are representative of those typically used in liquid chromatography. The Perkins and Johnston result, however, is a summary of experimental data for particulate beds with particles larger than typically used in chromatography. Also shown in Fig. 3 are the theoretical result of Tijssen [40] which assumes a random walk process where an eluite makes a random step in the radial direction each time it encounters a particle in its flow path, the theoretical result of Giddings [1] based on estimating the column length needed for two neighboring fluid elements to exchange positions in the radial direction, and the limiting value at high reduced velocities proposed by Tijssen and by Gunn [41] as the best fit to the existing experimental data, which is numerically equal to the Giddings result. Fig. 3 also illustrates an optimal correlation proposed in this study given by $Pe_r = 1/(1/20.4 + 0.75/v)$ which assumes that the effective radial dispersion coefficient is given by the sum of a molecular diffusion contribution corrected for the interparticle tortuosity and a convective dispersion contribution corresponding to a constant value for $D_r$. For the former contribution the values of $\gamma$ suggested by Tijssen when the interparticle porosity is 0.4 and

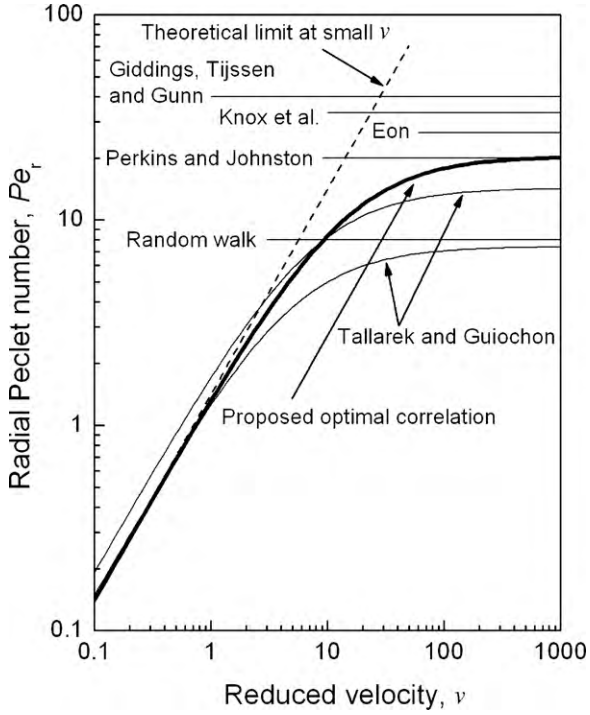


**Fig. 3.** Summary of relations describing the radial Peclet number as a function of the reduced velocity.

by Gunn were averaged, and for the latter contribution the various limiting values at large reduced velocities shown in Fig. 3 were averaged to yield an overall optimal value. Note finally that the vertical axis used in Fig. 3 corresponds to the value of $Pe_r$, where $Pe_r = 2/h_r$.

*2.1.2. The convection-only regime*

In contrast to the "close-to-equilibrium" regime discussed in the previous section, the "convection-only" regime considered in this section addresses the opposite situation where radial dispersion is absent and axial convection is the sole transport mechanism for the eluite. Consider an infinitely thin eluite band which is initially present at the location $z = 0$ when $t = 0$, and where the mass of eluite per unit area of column cross-section, defined as $m$, is constant across the column radius. The distance traveled by the eluite at the location $r$ after time $t$ is given by $z = u_f t$. If this relation is combined with the $n$th order velocity profile described in the previous section, the result can be solved for $r$ to yield:

$$r = \left(\frac{u_{f,cl} - z/t}{a u_{f,cl}}\right)^{1/n} R_c \tag{5}$$

where by definition $u_{f,cl} \geq z/t$.

Since radial mass transfer is assumed here to be absent, the mass of eluite present inside the column at the location $r$ in an annular ring of width $dr$ at any time is $2\pi r m dr$. This quantity is also the mass present in a column section of width $dz$ provided that $dz$ is chosen so that it contains the same eluite fraction as the $dr$ element just described. With $dz$ and $dr$ related in this way, it follows that

$$c_m^* \pi R_c^2 dz = -2m\pi r dr \tag{6}$$

where $c_m^*$ is the concentration of solute averaged across the column cross-section given by $c_m^* = 2\int_0^{R_c} c_m r dr / R_c^2$. Eliminating $r$ from Eqs. (5) and (6) yields

$$c_m^* = \frac{2m(t u_{f,cl} - z)^{(2-n)/n}}{(a t u_{f,cl})^{2/n} n} \tag{7}$$

For the case where $t$ is a constant, Eq. (7) yields the eluite concentration profile inside the column at a particular time. The second central moment of the band shape in terms of its spatial dimension, denoted as $\sigma_z^2$, can be determined using the relation

$$\sigma_z^2 = \frac{\int_{z_{min}}^{z_{max}} \pi R_c^2 c_m^* (z - z_{fm})^2 dz}{\pi R_c^2 m} \tag{8}$$

where $z_{fm}$ is the first absolute moment of the band shape given by $u_{f,ave} t$, and the limits of integration are $z_{min} = t u_{f,cl}(1 - a)$ and $z_{max} = t u_{f,cl}$. Eqs. (7) and (8) can be combined and integrated to yield $\sigma_z{}^2$, and by using the definition $H = \sigma_z^2 / L_c$ it then follows that

$$H_{CO} = \frac{a^2 n^2 L_c}{(n+1)(n+2-2a)^2} \tag{9}$$

Eq. (9) indicates that in the convection-only regime, the plate height is proportional to the column length, which agrees with experimental results obtained by some investigators under certain specialized conditions [16]. Substituting various values of $n$ into Eq. (9) for $n \geq 2$ indicates that $H_{CO}$ is relatively insensitive to the value of $n$ in this range. With $n = 2$ serving as a typical value, Eq. (9) reduces to

$$H_{CO,n=2} = \frac{a^2 L_c}{3(a-2)^2} \approx \frac{a^2 L_c}{12} \tag{10}$$

where the final approximate equality applies to small values of $a$ and results from taking the first term of a Taylor series expansion of the central expression in Eq. (10).

The results in this section are analogous to those of Vrentas and Vrentas [42] in their study of perturbation methods for the simple case of dispersion in an empty tube with laminar flow and where $a = 1$, and to those of Yun and Guiochon [43] who applied a numerical approach to a related problem involving nonlinear adsorption equilibrium. Additional details of the derivations given in this section as well as additional plate-height relations for the convection-only regime are given by Guo [44].

*2.1.3. The convection-only regime in terms of "mixing-cup" concentrations*

In the preceding section, the convection-only regime was described in terms of plate heights determined from statistical moments based on distances from the point of sample injection inside the column. It is of interest to also determine the corresponding relations based on the temporal concentration profile at the column exit, since this is generally the measurable quantity in chromatography experiments. For this purpose, it is necessary to distinguish between the area-average eluite concentration at the location $z$ and time $t$ inside the column defined previously, and the mixing-cup average concentration, denoted here as $c_m^\bullet$, which is defined to be the concentration which, when multiplied by the average fluid velocity, yields the axial eluite flux averaged across the column cross-section at the value of $z$ and $t$ under consideration. Consequently, it follows that

$$c_m^\bullet = 2\int_0^{R_c} \frac{c_m u_f r dr}{R_c^2 u_{f,ave}} \tag{11}$$

Eq. (11) has a particularly simple form in the present case where, at any location $z$ and time $t$, the eluite exists at only a single radial location $r$. If the fluid velocity at this location is denoted as $u_f$, it follows that

$$c_m^\bullet = \frac{c_m^* u_f}{u_{f,ave}} \tag{12}$$

Using the result for $c_m^*$ given by Eq. (7) it follows that for a specified value of $z$

$$c_m^\bullet = \frac{2m(tu_{f,cl} - z)^{(2-n)/n} z}{(atu_{f,cl})^{2/n} n u_{f,ave} t} \tag{13}$$

Plate heights determined from the eluite concentration profile as a function of time at the location $z$, with $z = L_c$ being the primary case of interest, can be determined by using the relation $H = \sigma_t^2 L_c / t_{fm}^2$ where

$$\sigma_t^2 = \frac{\int_{t_{min}}^{t_{max}} c_m^\bullet (t - t_{fm})^2 dt}{\int_{t_{min}}^{t_{max}} c_m^\bullet dt} \tag{14}$$

and

$$t_{fm} = \frac{\int_{t_{min}}^{t_{max}} c_m^\bullet t dt}{\int_{t_{min}}^{t_{max}} c_m^\bullet dt} \tag{15}$$

In Eqs. (14) and (15), $t_{max}$ and $t_{min}$ are the times when the eluite concentration decreases to zero and increases from zero, respectively, as given by $t_{max} = L_c/(u_{f,cl}(1-a))$ and $t_{min} = L_c/u_{f,cl}$. Upon performing the calculations described above for $n = 2$, i.e., for a parabolic velocity profile, it follows that

$$H_{CO} = L_c \frac{a^2 - (1-a)\ln(1/(1-a))^2}{(1-a)\ln(1/(1-a))^2} = \frac{a^2 L_c}{12} + \frac{a^3 L_c}{12} + \cdots \tag{16}$$

where the expression on the right side of the second equality in Eq. (16) results from taking the first two terms of a Taylor series expansion of the expression on the left side of that equality. Eq. (16) indicates that the plate height determined using mixing-cup concentrations is the same as that given by Eq. (10) for small $a$.

It is also of interest to investigate the eluite band shapes observed at the column exit as a function of time, i.e., the function $c_m^\bullet(t)$, for the convection-only regime as $n$ is varied. Note that $t$ has upper and lower limits of $t_{max}$ and $t_{min}$, and that $c_m^\bullet = 0$ for $t > t_{max}$ and $t < t_{min}$. Fig. 4 shows the concentration profiles for three different values of $n$. Although in practice these concentration profiles will be distorted by the other dispersion processes taking place, the results are nevertheless enlightening. For example, it can be seen that the concentration profile has a nearly rectangular shape when $n = 2$, while the concentration profile has fronting and tailing behavior when $n = 1$ and $n = 3$, respectively. This is consistent with the observation that fronting and tailing are commonly observed in chromatography even when the number of plates is large [45].

### 2.1.4. Extension of the Wang and Stewart theory

In addition to the "close-to-equilibrium" and "convection-only" cases discussed above, a more general theory can be developed based on an extension of the result of Wang and Stewart who analyzed convective dispersion in steady laminar flow through an empty tube [46]. To accomplish this, it is useful to first define the Fourier number as $\tau = D_r t / R_c^2$ where the characteristic time, $t$, is taken to be $L_c/u_{f,ave}$. Note that since the dimensional radial plate height is given by $H_r = 2D_r/u_{f,ave}$, the Fourier number can also be written as

$$\tau = \frac{H_r L_c}{2R_c^2} \tag{17}$$

As described by Wang and Stewart [46], for the case of convective dispersion in a cylindrical tube, the second central moment of an eluite band for any value of $\tau$ and for any velocity profile for the case where the band is present initially as an infinitely thin feed slug at the column entrance can be determinedby the following equation, which is based on a collocation method with two collocation points:

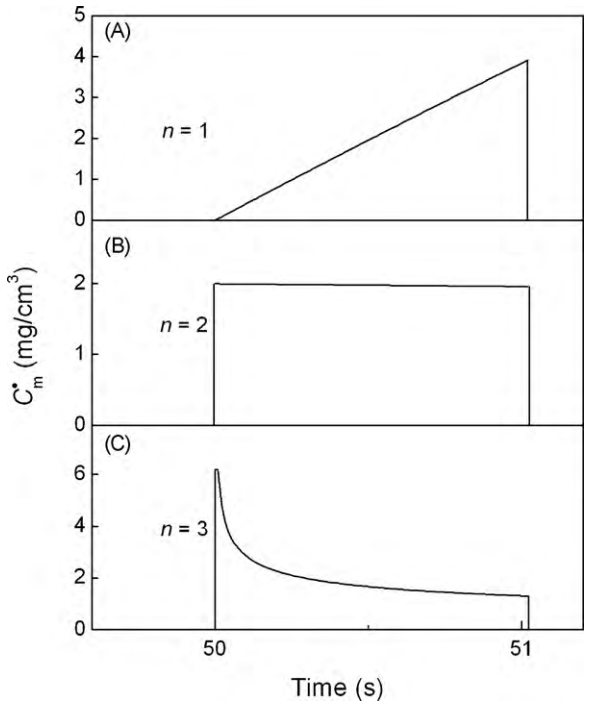


**Fig. 4.** Mixing-cup concentration at the column outlet for different flow profiles in the column. The flow profile is linear when $n = 1$, parabolic when $n = 2$, and cubic when $n = 3$. Conditions correspond to $L_c = 25$ cm, $a = 0.02$, $m = 1$ mg/cm$^2$, and $u_{f,cl} = 0.5$ cm/s.

$$\sigma_{WS}^2 = \left( \left( \frac{u}{u_{f,cl}} \right)_1 - \left( \frac{u}{u_{f,cl}} \right)_2 \right)^2 \left( \frac{\tau}{4} - \frac{1 - \exp(-16\tau)}{64} \right) \frac{u_{f,cl}^2 R_c^4}{8 D_r^2} \tag{18}$$

where the subscripts 1 and 2 denote the collocation points. Consider a quadratic profile where $(u/u_{f,cl})_i = 1 - a(r/R_c)_i^2$ and where $i$ represents the two collocation points and is either 1 or 2. The collocation points corresponding to the Gaussian nodes are [46]:

$$\left( \frac{r}{R_c} \right)_1^2 = \frac{1}{2} - \frac{1}{\sqrt{2}} \tag{19}$$

$$\left( \frac{r}{R_c} \right)_2^2 = \frac{1}{2} + \frac{1}{\sqrt{2}} \tag{20}$$

In addition, since $H_{WS} = \sigma_{WS}^2 / L_c$ and, for a quadratic profile, $u_{f,ave} = u_{f,cl}(1 - a/2)$, the above equations can be combined to yield:

$$H_{WS} = \frac{a^2}{(2-a)^2} \left[ \frac{R_c^2}{12 H_r} - \frac{R_c^4 (1 - \exp(-8 H_r L_c / R_c^2))}{96 H_r^2 L_c} \right] \tag{21}$$

Note that when $L_c$ is large, Eq. (21) reduces to $H_{WS} = a^2 R_c^2 / (12(2-a)^2 H_r)$ which is identical to the close-to-equilibrium result given by Eq. (4). Conversely, when $L_c$ is small, a Taylor series expansion yields $\exp(-8H_r L_c/R_c^2) \approx 1 - 8H_r L_c / R_c^2$ so that $H_{WS} = 0$ as expected. Eq. (21) also yields the result $dH_{WS}/dL_c\big|_{L_c=0} = a^2/(3(2-a)^2)$, which is the same value for $dH/dL_c$ given by the convection-only result using the first equality in Eq. (10). It is consequently interesting to compare $H_{CE}$, $H_{CO}$, and $H_{WS}$ since the preceding results show that $H_{WS}$ is asymptotic to both $H_{CE}$ and $H_{CO}$. Fig. 5 shows a comparison of the three theories plotted as $(2-a)^2 H/a^2$ versus $L_c$ for a particular choice of $h_r$, $d_p$, and $R_c$. Additional considerations related to the derivation and implications of Eq. (21) are given by Guo [44].

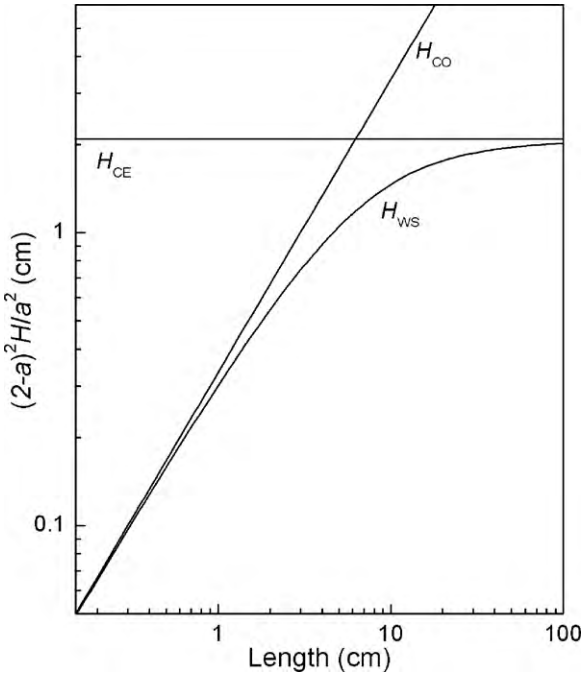


**Fig. 5.** Comparison of plate heights for the close-to-equilibrium ($H_{CE}$), convection-only ($H_{CO}$) and Wang and Stewart ($H_{WS}$) theories. Calculations correspond to $d_c = 0.1$ cm, $d_p = 10$ μm and $h_r = 0.1$.

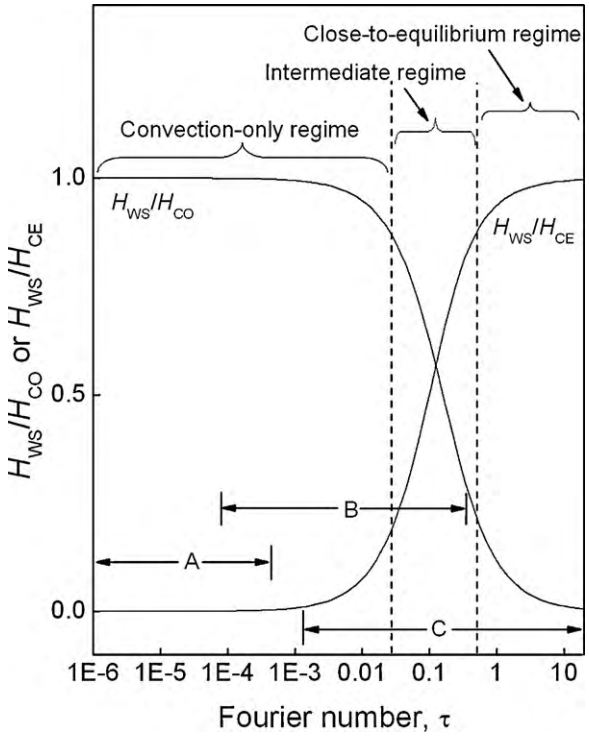


**Fig. 6.** Comparison of the ratios $H_{WS}/H_{CO}$ and $H_{WS}/H_{CE}$ as functions of the Fourier number. The Fourier number values characteristic of low-pressure process-scale chromatography, conventional HPLC, and microscale HPLC are denoted by the ranges A, B, and C, respectively.

Eq. (21) can be written in a convenient dimensionless form by defining the dimensionless column aspect ratio as $\lambda = L_c/R_c$ and the dimensionless column radius as $\psi = R_c/d_p$, and by replacing the radial plate height with $2d_p\psi\tau/\lambda$ to yield

$$h_{WS} = \frac{a^2\lambda\psi}{24(2-a)^2}\left[\frac{1}{\tau} - \frac{1-\exp(-16\tau)}{16\tau^2}\right] \quad (22)$$

Furthermore, since the Fourier number is related to the radial Peclet number by the relation $\tau = \lambda/(Pe_r\psi)$, and $Pe_r$ is a function of the reduced velocity, $\nu$, as shown in Fig. 3, Eq. (22) indicates that $h_{WS}$ can also be written as a function of $\nu$ with the quantities $a$, $\psi$, and $\lambda$ as function parameters. For the case when $\tau > 1$, the quantity in square brackets in Eq. (22) approaches the limiting value $1/\tau$ so that Eq. (22) becomes identical to the close-to-equilibrium result given by Eq. (4). Conversely, when $\tau < 0.01$, then the quantity in square brackets in Eq. (22) approaches the limiting value of 8 so that this equation becomes identical to the convection-only result given by the first equality in Eq. (10).

It is of interest to determine how the ratios $H_{WS}/H_{CO}$ and $H_{WS}/H_{CE}$ depend on the quantity $\tau$ since Eq. (22) indicates that these ratios are independent of $a$, $\lambda$, and $\psi$. Arguably, the three most prevalent categories of liquid chromatography are low-pressure process-scale chromatography, conventional-scale HPLC, and microscale HPLC. As a further generalization, the values of the column length vary from 20 to 50 cm, from 5 to 25 cm and from 5 to 25 cm for these three scales respectively, the values of the particle diameter vary from 50 to 100 μm, from 2 to 10 μm and from 2 to 10 μm for these three scales respectively, and the values of the column radius vary from 10 to 100 cm, from 0.1 to 0.23 cm, and from 0.01 to 0.1 cm for these three scales, respectively. Assuming that the reduced radial plate height varies in practice from 0.05 to 0.1 as shown in Fig. 3, then Eq. (17) indicates that these various parameter ranges yield corresponding ranges in τ, as shown in Fig. 6. This figure also illustrates the relation between $H_{WS}/H_{CO}$, $H_{WS}/H_{CE}$, and $\tau$, and indicates that, as a general rule, for process-scale chromatography the transcolumn contribution to dispersion is in the convection-only regime, while for conventional-scale HPLC the transcolumn contribution to dispersion can be in either the convection-only or intermediate regimes. Fig. 6 also indicates that for microscale HPLC the transcolumn contribution to dispersion can be in all three regimes.

### 2.2. Approximate Fourier numbers for the various intracolumn dispersion domains

In order to properly interpret results presented in the experimental section of this study, it is useful to determine approximate Fourier number values for the various intracolumn dispersion domains by employing Eq. (17). As pointed out by Giddings [1], the complete fluid flow pattern inside a chromatography column can be considered as the superposition of individual domains of various scales, with the dispersion phenomena occurring in each domain taking place largely in an independent manner. It therefore follows that although the results in Section 2.1.1 were developed specifically for the transcolumn domain, they can be applied directly to the other domains that exist. For this purpose a dimensionless characteristic length and radius for the individual subdomains of a particular domain can be defined as $\omega_\lambda = l_{domain}/d_p$ and $\omega_\alpha = r_{domain}/d_p$. Using the first parameter, the Fourier number can be related to the number of diffusional jumps, $n_D$, defined by Giddings [1] as follows

$$n_D = \frac{2l_{domain}D_r}{u_{f,ave}\omega_\alpha^2 d_p^2} = 2\tau \quad (23)$$

Note that the second equality in Eq. (23) results from Eq. (17) and that the expression on the right side of the first equality in Eq. (23) is the expression given by Giddings for $n_D$ except that $D_r$ is used in place of $D_m$.

Since $Pe_r = u_{f,ave}d_p/D_r$, the second equality in Eq. (23) can be rearranged to yield $\tau = \omega_\lambda/(\omega_\alpha^2 Pe_r)$. Although correlations for radial dispersion analogous to the proposed optimal correlation in Fig. 3

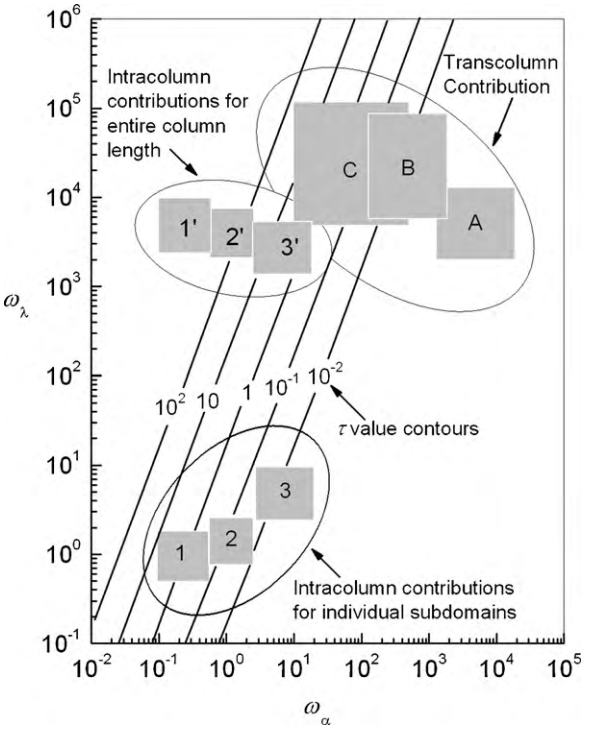


**Fig. 7.** Location of different dispersion contributions on a contour plot of the Fourier number as a function of $\omega_\lambda$ and $\omega_\alpha$. A denotes the transcolumn contribution in low-pressure process-scale chromatography, B denotes this contribution in conventional HPLC, and C denotes this contribution in microscale HPLC. 1, 2, and 3 denote the transchannel, short-range interchannel, and long-range interchannel contributions for single subdomains, respectively, as defined by Giddings [1]. 1′, 2′, 3′ denote the transchannel, short-range interchannel, and long-range interchannel contributions for the entire column length.

are currently not available for the various intracolumn dispersion domains identified by Giddings, it is reasonable to expect that Fig. 3 applies at least qualitatively to these domains. Furthermore, in most practical chromatography processes the reduced velocity is in the range $10 < \nu < 1000$, in which case Fig. 3 implies that $10 < Pe_r < 20$, and it can therefore be expected that $\tau \approx \omega_\lambda/(15\omega_\alpha^2)$, which represents an average value of $\tau$ for the case considered here.

Fig. 7 illustrates the value of the Fourier number determined using the expressions just described for the transcolumn contribution to convective dispersion for the different categories of chromatographic processes mentioned earlier. This figure also illustrates the value of the Fourier number determined similarly for the transchannel, short-range interchannel, and long-range interchannel contributions using the ranges of values for $\omega_\lambda$ and $\omega_\alpha$ suggested by Giddings [1]. Note that Fig. 7 shows both the Fourier number for the individual subdomains for each intracolumn contribution and the Fourier numbers for the intracolumn contributions corresponding to the entire column length given by the product of the Fourier number for the individual subdomains and the number of subdomains encountered by an eluite as it travels through the column based on estimates of the number of subdomains present in columns of typical lengths containing particles of typical diameters. As shown in Fig. 7, this analysis indicates that it is reasonable to assume that the Fourier number is large for all the intracolumn contributions to convective dispersion, and that the close-to-equilibrium regime consequently applies to these contributions.

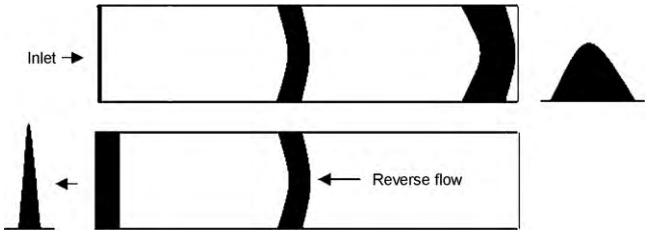


**Fig. 8.** Illustration of band broadening processes inside a chromatography column for conventional and bi-directional plate-height experiments.

### 2.3. Implication for bi-directional plate-height experiments

As discussed earlier, in a bi-directional plate-height experiment the feed sample is initially injected into the column inlet as a thin band. For the case where the transcolumn contribution to dispersion is significant, and where the convection-only regime applies to this contribution, then as the band travels from where it was injected to the other end of the column it becomes increasingly "crescent shaped" as illustrated in Fig. 8. However, if the fluid velocity at each radial position everywhere in the column reverses its direction but maintains the same magnitude when the flow direction is reversed, then this crescent shape decreases in magnitude and eventually disappears completely after the flow direction is reversed and the band reaches the original column entrance, as also illustrated in Fig. 8.

For the case where the transcolumn contribution to dispersion is in the convection-only regime and is therefore characterized by a small Fourier number (i.e., $\tau < 0.01$), the width of the band when it exits the column in a bi-directional plate-height experiment results from the contribution from the original band width, the contribution from molecular diffusion, and the intracolumn contributions to dispersion since these last contributions are generally always characterized by large Fourier numbers (i.e., $\tau > 1$). The case where the transcolumn contribution is characterized by moderate to large Fourier numbers (i.e., $\tau > 0.01$) is more complex however since, even in the absence of molecular diffusion or an intracolumn contribution to dispersion, the radial transport that occurs in this regime produces a local broadening of the eluite band at any given radial position that does not become smaller when the flow direction is reversed.

In order to develop relations for interpreting bi-directional plate-height experiments in the moderate to high Fourier number regime that apply to the transcolumn contribution, it is necessary to compare theoretically the width of the entire band with the local width of the band at the position $r$. By definition, the concentration profile for a Gaussian band shape is given by

$$c_m^* = c_{m,max}^* \exp\left(\frac{-(z - z_{max})^2}{2\sigma_{total}^2}\right) \tag{24}$$

where $\sigma_{total}$ is the standard deviation of the peak shape and $z_{max}$ is the location of the maximum value of $c_m^*$, denoted as $c_{m,max}^*$. If $\Omega$ is the deviation from radial diffusional equilibrium defined as $\Omega = c_m/c_m^* - 1$, it follows that

$$c_m = c_{m,max}^* \exp\left(\frac{-(z - z_{max})^2}{2\sigma_{total}^2}\right)(1 + \Omega) \tag{25}$$

According to the generalized nonequilibrium theory of Giddings, the $r$ functionality of $\Omega$ can be determined by solving the equation [1]

$$\frac{1}{r}\frac{d}{dr}r\frac{d\Omega}{dr} = (u_f - u_{f,ave})\frac{d\ \ln(c_m^*)}{D_r dz} \tag{26}$$

subject to the boundary conditions that $d\Omega/dr = 0$ at $r = R_c$ and $\int_0^{R_c} r\Omega dr = 0$. Note that the quantity $d \ln c_m^*/dz$ in Eq. (26) is not a function of $r$, and its dependence on $z$ can be determined from

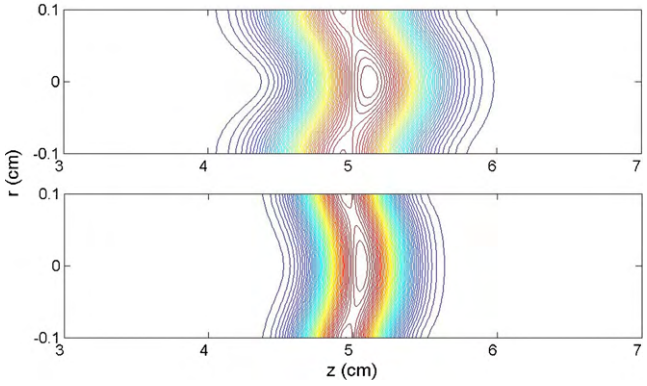


**Fig. 9.** A contour plot of the eluite concentration as a function of radius and axial position as given by Eq. (28). Conditions correspond to $z_{max} = 5$ cm, $c^*_{m,max} = 0.1$ mg/ml, $u_{f,cl} = 0.05$ cm/s, $R_c = 0.1$ cm, $d_p = 0.001$ cm, $h_r = 0.1$ and $a = 0.1$ for both panels. Panel A: $n = 2$, $\sigma_{total} = 0.32$ cm; Panel B: $n = 10$, $\sigma_{total} = 0.21$ cm. Red: 0.06 mg/ml < $c_m$ < 0.1 mg/ml; blue: 0.0 mg/ml < $c_m$ < 0.04 mg/ml. (For interpretation of the references to color in this figure legend, the reader is referred to the web version of the article.)

Eq. (25). Solving for $\Omega$ using the above relations for the case of a quadratic velocity profile where $u_f = u_{f,cl}(1 - ar^2/R_c^2)$ yields

$$\Omega = \frac{au_{f,cl}(z - z_{max})(3r^4 - 6r^2R_c^2 + 2R_c^4)}{48D_rR_c^2\sigma^2_{total}} \tag{27}$$

Substituting from above yields the final result for $c_m$ as a function of $z$ and $r$ as follows:

$$c_m = c^*_{m,max}\ \exp\left(-\frac{(z - z_{max})^2}{2\sigma^2_{total}}\right) \times \left(1 + \frac{au_{f,cl}(z - z_{max})(3r^4 - 6r^2R_c^2 + 2R_c^4)}{48D_rR_c^2\sigma^2_{total}}\right) \tag{28}$$

Fig. 9 illustrates the two-dimensional eluite concentration profile determined from Eq. (28) for two different values of $n$ and for a particular selection of physical parameters as described in the figure caption corresponding to $\tau = 0.1$.

Since radial dispersion in the presence of a radial variation in axial fluid flow yields random walk behavior for individual eluite molecules in the axial direction regardless of the shape of the concentration profile that exists for the eluite [1], it follows that the local variance of the eluite band shape (i.e., the second central moment of the band shape) in the axial direction at the location $r$ increases in proportion to the length traveled by the eluite band regardless of whether or not the flow direction is reversed. If the local band variance at the location $r$ is therefore written as $\sigma^2_{nr}$ to denote that it is "nonreversible" with respect to changes in the flow direction, then the ratio $\sigma^2_{nr}/\sigma^2_{total}$, where $\sigma^2_{total}$ is the total band variance considering the entire two-dimensional shape of the band, can be interpreted as the fraction of the total variance observed in a conventional plate-height experiment due to the local width of the peak at the location $r$. Consequently, $\sigma^2_{nr}/\sigma^2_{total}$ can also be interpreted as the ratio of variances that would be observed when comparing a bi-directional plate-height experiment and a conventional plate-height experiment if the eluite travels the same distance in both cases.

An especially simple result for $\sigma^2_{nr}/\sigma^2_{total}$ can be developed if it is assumed that the shape of the eluite band at the local position $r$ is Gaussian, in which case the value of $\sigma^2_{nr}$ at a certain location $r$ is given by the negative of the second derivative in the $z$ direction of the eluite concentration at its maximum value. Applying this approach and using Eq. (28) yields the following result:

$$\frac{\sigma^2_{nr}}{\sigma^2_{total}} = \frac{1}{2} + \frac{12D_rR_c^2\sigma_{total}}{[a^2u^2_{f,cl}(3r^4 - 6r^2R_c^2 + 2R_c^4)^2 + 576D_r^2R_c^4\sigma^2_{total}]^{1/2}} \tag{29}$$

Since $\sigma_{nr}$ varies with $r$, the effective average value of $\sigma_{nr}$ for the eluite band must be determined by integrating Eq. (29) across the column radius. However, since this integral does not have a simple analytical form, and since the eluite mass concentration is not necessarily uniform across the column radius depending on how the sample is originally injected, it is generally preferable to determine $\sigma_{nr}$ for various radial positions, and to then average these values as appropriate for the problem at hand. For example, for the particular case when $r = 0$, Eq. (29) becomes

$$\frac{\sigma^2_{nr}}{\sigma^2_{total}} = \frac{1}{2} + \frac{12D_rR_c^2\sigma_{total}}{(4a^2u^2_{f,cl}R_c^8 + 576D_r^2R_c^4\sigma^2_{total})^{1/2}} \tag{30}$$

From the definition $H = \sigma^2/L$, it follows that $\sigma^2_{total} = HL_c$. Combining this result with Eq. (4) yields

$$\sigma_{total} = \frac{aR_c}{12}\sqrt{\frac{3L_c}{H_r}} \tag{31}$$

If the relation $H_r = 2R_c^2\tau/L_c$, where $\tau$ is the Fourier number, is combined with the defining relation $H_r = 2D_r/u_{f,ave}$, then substitutions using Eqs. (30) and (31) yields

$$\left(\frac{\sigma^2_{nr}}{\sigma^2_{total}}\right)_{r=0} = \frac{1}{2}\left(1 + \sqrt{\frac{3\tau}{3\tau + 2}}\right) \tag{32}$$

By using the same procedure, it follows that for $r = R_c/2$

$$\left(\frac{\sigma^2_{nr}}{\sigma^2_{total}}\right)_{r=R_c/2} = \frac{1}{2}\left(1 + \sqrt{\frac{127\tau}{127\tau + 10}}\right) \tag{33}$$

and for $r = R_c$

$$\left(\frac{\sigma^2_{nr}}{\sigma^2_{total}}\right)_{r=R_c} = \frac{1}{2}\left(1 + \sqrt{\frac{6\tau}{6\tau + 1}}\right) \tag{34}$$

The above results indicate that at most one half of the total bandwidth, as measured by $\sigma^2_{total}$, is eliminated when the flow direction is reversed in a bi-directional plate-height experiment, and that this limit occurs when $\tau$ is small. However if $\tau$ is very small, then the close-to-equilibrium mechanism used here becomes invalid, and the convection-only mechanism applies. Consequently, to arrive at an approximate relation that applies to all values of $\tau$, it is reasonable to first average as appropriate the results given by Eqs. (32)–(34) for the close-to-equilibrium regime to arrive at a representative value for $\sigma_{nr}$ characteristic of the entire eluite band, and to then average that result with the result $\sigma^2_{nr} = 0$ that applies to the convection-only regime using the weighting factor $H_{WS}/H_{CE}$ (or equivalently the factor $1 - H_{WS}/H_{CO}$) which describes the relative importance of each ideal regime in this intermediate Fourier number range (see Fig. 6). Consequently, it will be assumed over the entire Fourier number range that $\sigma^2_{nr}/\sigma^2_{total} \approx (H_{WS}/H_{CE})(\sigma^2_{nr}/\sigma^2_{total})_{CE}$, where the subscript "CE" denotes the result assuming that the close-to-equilibrium regime applies.

In addition to describing bi-directional plate-height experiments, the relations in this section can also be used to gain additional insights into the dispersion phenomena occurring inside a chromatographic column. In particular, Fig. 10A shows how the local band variance varies in the radial direction inside a column according to Eq. (29). As shown in the figure, the value of $\sigma^2_{nr}$, or equivalently the local plate height at the location $r$, is a minimum at the column center, increases to its maximum value at

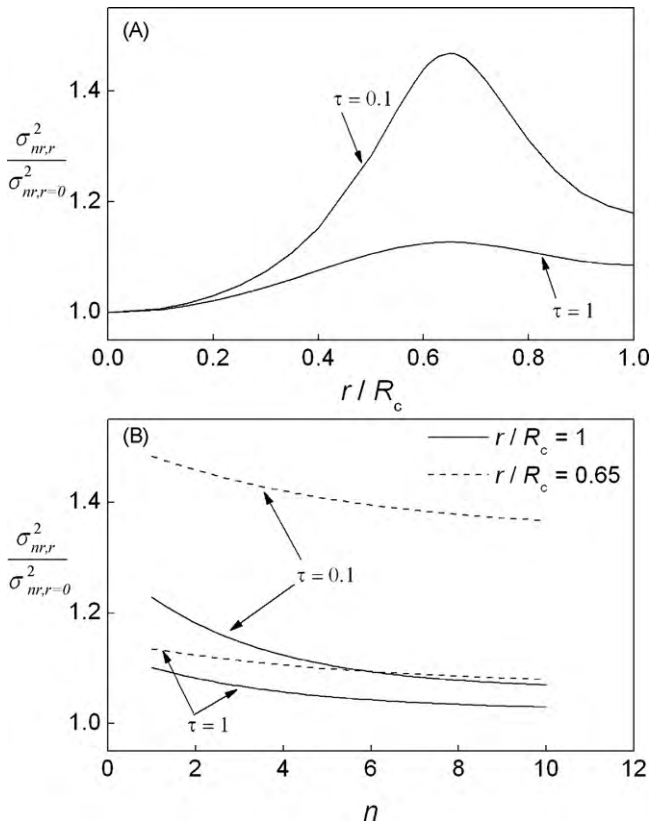


**Fig. 10.** Illustration of the local band variance inside the column. Panel A shows the variation in the local band variance as a function of $r/R_c$ for two different Fourier numbers, and for a parabolic velocity profile where $n = 2$. Panel B shows the ratio of the local band variance at the column wall to the local band variance at the column center, and the local band variance at $r/R_c = 0.65$ to the local variance at column center as functions of the parameter $n$ in Eq. (2). The value $r/R_c = 0.65$ corresponds approximately to the maximum value of the local band variance for the range of $n$ values shown.

approximately $r/R_c = 0.65$, and then decreases as the column wall is approached. This is consistent with the experimental results of Abia et al. [47] who, at the approximate Fourier number of 0.1 measured local plate heights inside a chromatographic column and found that the plate height was smallest at the column center and that the plate height increased by a factor of approximately 1.5 as the wall was approached. Similarly, Fig. 10B shows how the ratio of $\sigma^2_{nr}$ at the column wall and at the column center varies when the velocity profile is varied, as described by the value of $n$ for two different values of $\tau$. As illustrated in the figure, this ratio approaches unity at large $n$, which is consistent with the characteristic that large values of $n$ correspond to plug flow of fluid in the column (see Fig. 2A).

## 3. Experimental

### 3.1. Materials and chemicals

The four columns used were an in-house packed 12.3 cm × 1.0 cm I.D. Omnifit column (Bio-Chem Fluidics, Boonton, NJ, USA) containing 85-μm solid glass particles obtained from Potters Industries (Valley Forge, PA, USA), an in-house packed 10 cm × 0.46 cm I.D. PEEK column (manufactured by Perseptive Biosystems, now Applied Biosystems, Foster City, CA, USA) containing 7-μm solid glass particles also obtained from Potters Industries, a 25 cm × 0.4 cm I.D. PROPAC WAX-10 column packed with 10-μm nonporous polystyrene particles (Dionex, Sunnyvale, CA, USA), and a 10 cm × 0.46 cm I.D. Mono Q column packed with 10-μm polystyrene porous particles (GE Healthcare, Piscataway, NJ, USA).

Gly-Gly-Tyr-Arg, Trp-Gly, β lactoglobulin B, Trisma base, NaCl, HCl and fluorescene were obtained from Sigma (St. Louis, MO, USA). All solutions were prepared by vacuum filtering using a 0.2 μm pore size nylon membrane filter (Whatman, Sanford, ME, USA). Each feed sample was dissolved into filtered buffer solution and then filtered again with a PVDF syringe driven filter with 0.2 μm pore size (Whatman, Sanford, ME, USA).

### 3.2. Instrument

Isocratic experiments were performed using an Ultimate HPLC instrument (Dionex, San Francisco, CA, USA). A microbore flow cell with a volume of 2 μl was used in order to minimize dispersion resulting from the detector flow cell. A Rheodyne Model 9010 valve (Rheodyne, Rohnert Park, CA, USA) was used for flow reversal. Black PEEK tubing with 100 μm I.D. was purchased from Upchurch Scientific (Oak Harbor, WA, USA). To minimize the extra-column band broadening, the length of tubing used was made as short as possible. An Orion 520A pH meter (Orion, Beverly, MA, USA) was used to measure the pH when making buffers.

The system dead volume and extra-column dispersion were determined by replacing the column with a low-dead-volume union, and then measuring both the elution time for an eluite to pass through the system and the effluent concentration profile of the eluite. In the conventional van Deemter experiments, the extra switching valve was absent, and the dead volume for the HPLC system without this valve was determined to be 18 μl. The dead volume in the bi-directional experiments was 40 μl due to the presence of the additional switching valve.

A Model 1666 HPLC column Slurry Packer from Alltech (now Grace Davison, Columbia, MD, USA) was used for the high-pressure slurry packing of columns. This instrument employs a pneumatic amplification pump with an amplification ratio of 1:100 so that the pressure generated by the pump is about 100 times the air pressure applied.

### 3.3. Methods

The Omnifit column and the PEEK column were packed by a low-pressure slurry packing method and a high-pressure slurry packing method respectively. The low-pressure slurry packing method consisted of first suspending the glass particles in filtered 20% (v/v) ethanol to make a slurry, then introducing the slurry into the column held in a vertical position with the bottom frit and column end piece installed. After an initial period of gravity settling, the bed was then further consolidated by subjecting it to flow using 20% (v/v) ethanol at 40 bar for 4 hours. The column inlet end piece containing the inlet frit was then attached to the column. In the high-pressure slurry packing method, the slurry was first introduced into the high-pressure slurry reservoir (manufactured by Perseptive Biosystems, now Applied Biosystems, Foster City, CA, USA) which was connected to the column, and the driving solvent consisting of 50% (v/v) methanol was then pumped through the reservoir and column at 350 bar for 3 hours using the pneumatic amplification pump. The pump was then turned off so that the system could be depressurized to atmospheric pressure, and the column end fittings and frits were then quickly attached.

As described earlier, a bi-directional chromatographic setup as shown in Fig. 11 was used to discriminate between the intracolumn and the transcolumn dispersion contributions. The bi-directional experiments were operated in two stages. In the first stage, different eluites were injected and then allowed to pass through the column to the column midpoint as determined by comparing the elution time with the total elution time for the eluite to travel

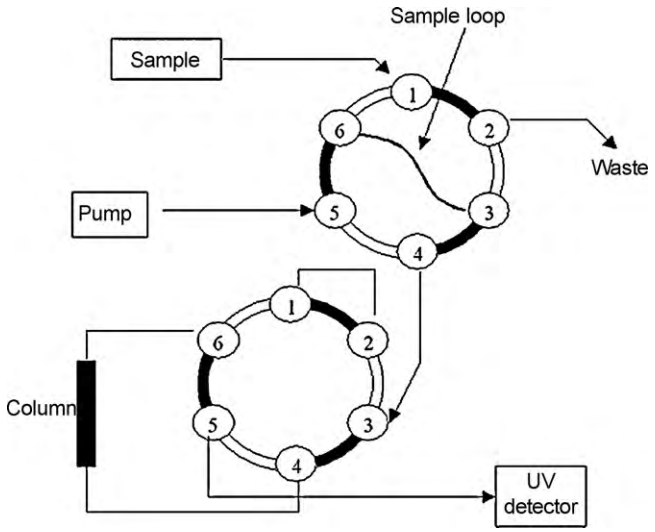


**Fig. 11.** Schematic of the bi-directional experiments. The upper 6-port valve is the sample injection valve and the lower 6-port valve is the switching valve. The flow direction is $1 \rightarrow 6 \rightarrow 3 \rightarrow 2$ in the loading position, and the flow direction is $5 \rightarrow 6 \rightarrow 3 \rightarrow 4$ in the injection position. For the forward-directional experiments, the fluid travels in the path $3 \rightarrow 2 \rightarrow 1 \rightarrow 6 \rightarrow$ column $\rightarrow 4 \rightarrow 5 \rightarrow$ dector, while in the bi-directional experiments the fluid travels in the path $3 \rightarrow 4 \rightarrow$ column $\rightarrow 6 \rightarrow 5 \rightarrow$detector.

through the column. When the eluite reached the position of interest inside the column, the direction of flow in the column was reversed using the switching valve.

### 3.4. Data processing

Chromeleon chromatography management software version 6.6 was used together with the Ultimate HPLC system to determine the bandwidth at the band half height and the band asymmetry factor at 10% of the band height. The band shape was then assumed to be described by an exponentially modified Gaussian (EMG) function, and the EMG-based equations described by Foley and Dorsey [48] were used to determine the number of theoretical plates and the plate height so that peak asymmetry was accounted for.

In order to increase the accuracy of the bi-directional plate-height experiments, these experiments were conducted from both ends of the column with the eluite band direction reversed when the band was at the column midpoint. This method was considered to be more accurate than a bi-directional plate-height experiment conducted from a single column end since in the former method the eluite band encounters both column end frits, and since for the latter method it is difficult to make sure the eluite band travels the entire column length in both directions without some portion of the band leaving the column, which would likely alter the band shape. If the number of plates measured by the two bi-directional plate-height experiments each involving one half of the column length and each starting from opposite column ends are denoted as $N_1$ and $N_2$, which are generally unequal due to axial variations in column properties, then since $N_1 = (L_c/2)^2/\sigma_1^2$ and $N_2 = (L_c/2)^2/\sigma_2^2$, and since the number of plates that would be measured by a hypothetical single bi-directional plate-height experiment that involved the entire column length is given by $N = L_c^2/(\sigma_1^2 + \sigma_2^2)$, it follows that $N = 4/(1/N_1 + 1/N_2)$.

As mentioned earlier, the band variance from extra-column sources was measured by replacing the column by a low-dead-volume union, and then determining the eluite band shape that results from a sample injection. This quantity was then subtracted from the total variance for the conventional plate-height experiments so that the band broadening resulting solely from dispersion processes inside the column could be determined. Experiments of this type are termed here "conventional" plate-height experiments. However, for the case of the bi-directional plate-height experiments, the extra-column band broadening was not subtracted from the measured band variance since bi-directional experiments were always compared only to an experiment which also incorporated the extra switching valve but where flow reversal was not performed. These two types of experiments, termed here the "bi-directional" and "forward-directional" experiments, respectively, incorporated essentially the same amount of extra-column dispersion so that, when the band variances from these two experiments were subtracted, the extra-column contribution effectively cancels from the result.

In order to preserve the bed structure when reversed flow was used in the column, bi-directional plate-height experiments were performed at low flow rates, e.g., less than 0.15 $cm^3$/min for a standard size HPLC column where $d_c = 0.46$ cm. The low flow rates used also ensured that temperature gradients inside the column produced by viscous dissipation were minimal. In particular, it has been shown recently by Fallas et al [49] that plate heights are affected by the temperature gradients produced by viscous dissipation inside a chromatographic column only when relatively small particles (e.g., $d_p < 5$ μm) are employed at high flow rates. Furthermore, because the bi-directional plate-height experiments would have been difficult to perform in a fully thermostated system due to the extra switching valve present and because of the need for fluid pre-heaters at both column ends, it was judged preferable to carry out the experiments with the column suspended in open air. To further confirm that temperature gradients inside the column were not a critical factor in the experiments performed, in a limited number of experiments a fan was used to blow air across the column to alter the heat-transfer coefficient between the column and the surrounding air. Plate heights measured under these conditions were compared with plate heights measured in identical experiments but with the column suspended in still air, and it was determined that there was no significant difference between these two cases.

## 4. Results and discussion

Fig. 12A illustrates results for a new Dionex ProPac WAX-10 column containing nonporous particles which indicate that plate heights measured in the conventional experiment under conditions of no eluite retention agree well with the most common version of the original Knox equation with the $C$ term for intraparticle diffusion eliminated, as given by $h = B/\nu + A\nu^{1/3}$ with $A = 1$ and $B = 2$ [3,4]. Note that at low reduced velocities the plate heights in both the upper and lower panels in Fig. 12 decrease as the reduced velocity increases due to the presence of molecular diffusion, which is represented by the $B$ term of the Knox equation. Fig. 12B also indicates that the reduced plate height for the forward-directional plate-height experiment is approximately 25% greater than for the bi-directional experiment. Furthermore, the Fourier number, $\tau$, determined using Eq. (17) and the proposed optimal correlation for radial dispersion given in Fig. 3 is 0.093 when the flow rate is 0.06 $cm^3$/min, which corresponds to $\nu = 7.2$. From Fig. 6 it can be seen that this value for $\tau$ corresponds to the intermediate transport regime. As discussed in Section 2.3, under these conditions the transcolumn contribution to convective dispersion can be determined by dividing the plate-height difference between the forward and bi-directional experiments by factor $1 - \sigma_{nr}^2/\sigma_{total}^2$, where $\sigma_{nr}^2/\sigma_{total}^2 \approx (H_{WS}/H_{CE})(\sigma_{nr}^2/\sigma_{total}^2)_{CE}$, and where $(\sigma_{nr}^2/\sigma_{total}^2)_{CE}$ can be determined by averaging the three results given by Eqs. (32)–(34).

Fig. 12A shows the theoretically predicted transcolumn plate-height contribution calculated using Eq. (21) assuming that the

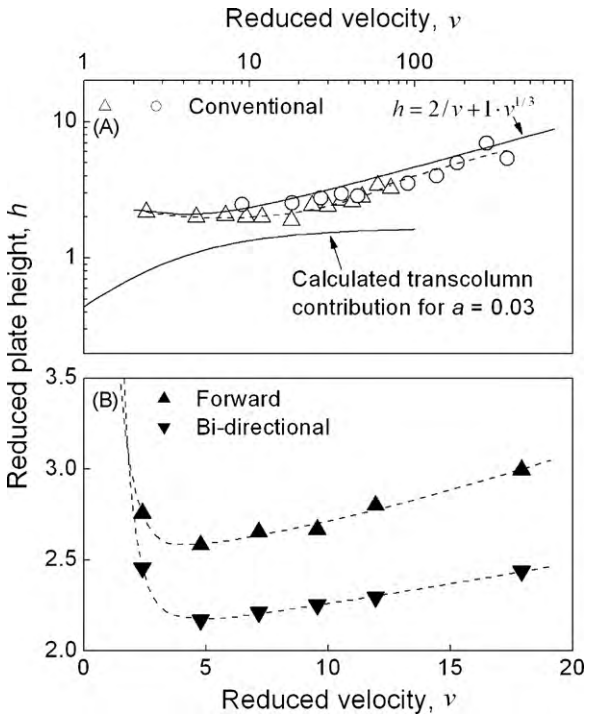


**Fig. 12.** Results from conventional, forward, and bi-directional plate-height experiments using a new PROPAC WAX-10 column for an unretained eluite. The feed sample consisted of 2 μl of either 1 mg/ml tetrapeptide (Gly-Gly-Tyr-Arg) or 1 mg/ml of β lactoglobulin B. Mobile Phase: 20 mM Tris, 0.2 M NaCl, pH 9. Dashed curves shown are fits to the empirical Knox equation given by $h = (1/A + 1/(Dv^n))^{-1} + B/v + Cv$. Bi-directional experiments were performed using the tetrapeptide. Conventional experiments using the tetrapeptide and β lactoglobulin B are denoted by the open triangles and the open circles, respectively.

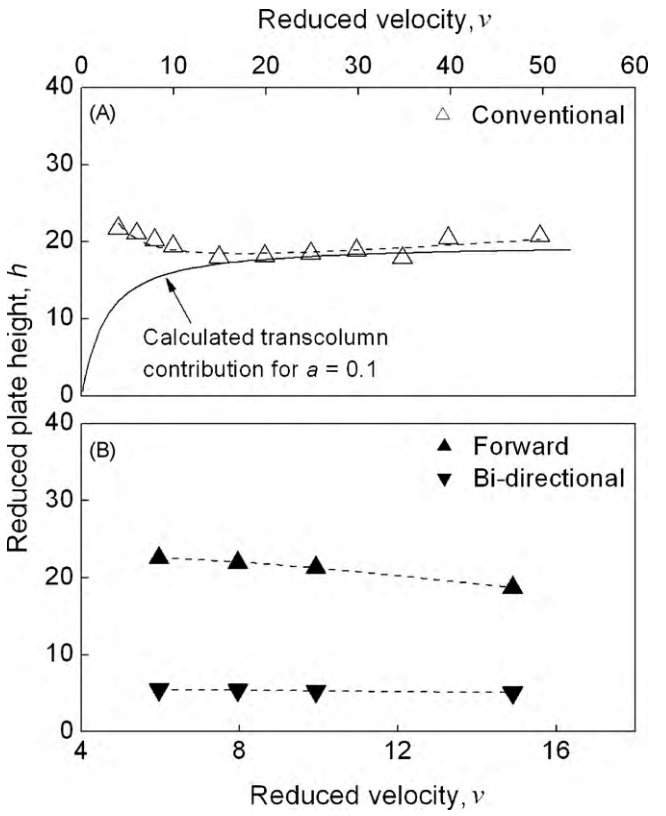


**Fig. 13.** Results from conventional, forward, and bi-directional plate-height experiments using the aged PROPAC WAX-10 column for an unretained eluite. The feed sample consisted of 2 μl of 1.0 mg/ml dipeptide (Trp-Gly). Mobile Phase: 20 mM Tris, 0.2 M NaCl, pH 9. Dashed curves shown are fits to the empirical Knox equation given by $h = (1/A + 1/(Dv^n))^{-1} + B/v + Cv$.

radial plate height is given by the proposed optimal correlation in Fig. 3 and assuming $a = 0.03$, which is the best fitting value of $a$ as determined from the difference between the forward and bi-directional experimental data in Fig. 12B. The results shown indicate that the transcolumn contribution to convective dispersion constitutes somewhat less than one half of the total amount of eddy dispersion present. Fig. 12A also indicates that the theoretically predicated plate height for the transcolumn contribution increases at a slower rate with the reduced velocity than the experimental data. This is most likely because of either imprecisions in the shape of the proposed correlation for $Pe_r$ in Fig. 3 at higher reduced velocities, or because the intracolumn contributions to dispersion increase substantially at higher reduced velocities, possibly because of the transition from laminar to turbulent flow in the interparticle interstices as the flow rate is increased. Finally, it can be observed that the value of $a$ determined in Fig. 12B corresponds to the lowest range of axial velocity variations across the column diameter measured directly in past studies [26], which indicates that this column as supplied by the manufacturer is nearly optimally packed.

Fig. 13 shows results for the same column used in Fig. 12, but after this column was subjected to more than one thousand sample injections over the course of one year, including a significant number of bi-directional plate-height experiments where flow reversal can be expected to adversely affect the particle bed structure in the column. As shown in Fig. 13A, the plate heights for this "aged" column are higher than those for the same column when it was new. The same procedure as described above was used to calculate the transcolumn plate height, and the best fitting value of $a$ was determined to be 0.1, which indicates that the radial variation in axial fluid velocity is significantly larger in the aged Dionex column. It can also be seen in Fig. 13 that the theoretically predicted plate heights from the transcolumn contribution using the value $a = 0.1$ in Eq. (21) are almost equal to the actual plate heights measured in the conventional plate-height experiment, which indicates that the column aging process yields a greater transcolumn contribution to the total amount of convective dispersion as opposed to an increase in the intracolumn contributions.

Fig. 13 also indicates that the difference between the forward and bi-directional plate-height measurements for the aged Dionex column are greater than one half of the conventional plate-height result. This is consistent with the calculated Fourier number of 0.093 since, according to Fig. 6, this value for the Fourier number indicates that the column is operating in the intermediate regime and not in the close-to-equilibrium regime. According to Eqs. (32)–(34), if the column is operated in the close-to-equilibrium regime, then the difference between plate heights determined from the forward and bi-directional plate-height experiments can be at most one half of the plate height from the conventional experiments.

Fig. 14 illustrates a comparison of band shapes for a forward-directional plate-height experiment and its reverse-flow counterpart for the case of the aged Dionex column where unretained eluite conditions were employed. It can be observed in the figure that the eluite band is narrower and more symmetrical in the bi-directional experiment in comparison to the forward-directional experiment. Note that the greater band asymmetry in Fig. 14 for the forward-directional experiment is consistent with the band shape predicted by the "convection-only" mechanism with $n > 2$ as discussed in Section 2.1.3. More specifically, even though the forward-directional result corresponds to a reasonably

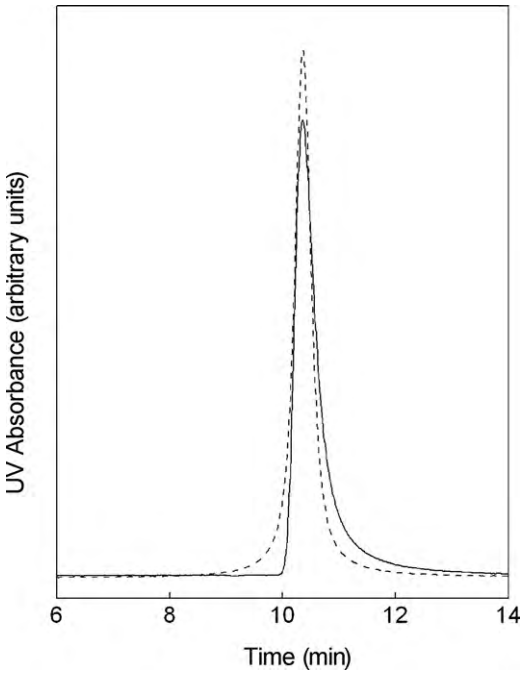


**Fig. 14.** Comparison between forward and bi-directional experiments, where the direction of flow was reversed when the peak was halfway through the column. For comparison purposes, the absorbance scales are different for the two results so that the two eluite bands have the same area. Forward: ——; Bi-directional: - - - -.

large plate number of $N = 1400$, the band is nevertheless asymmetrical in shape, which suggests that the convection-only regime described in Section 2.1.2 plays a significant role in determining the bandwidth.

Fig. 15 shows results from plate-height experiments performed using an in-house packed Omnifit column containing 85-μm solid glass particles under conditions of no eluite retention. It can again be observed, as in Fig. 13, that the difference in the plate heights between the forward and bi-directional experiments is almost equal to the plate height obtained in the conventional plate-height experiments shown in Fig. 15B, which indicates that almost all the band broadening measured in the conventional experiments comes from the transcolumn contribution to convective dispersion. The large difference between the results for the forward and bi-directional plate-height experiments is also consistent with being in the convection-only regime, as further indicated by the relatively low Fourier number of 0.03 that applies, as determined using Eq. (17). Finally, by using the same procedure as described above, the value of $a$ determined in Fig. 15B is 0.18 which, although a comparatively large value, is still within the range of values obtained in other studies of similar types of columns where the variation in axial fluid velocity across the column radius was determined using NMR tomography [50].

Bi-directional plate-height experiments were also performed using a column containing porous particles as shown in Fig. 16. The difference observed in the reduced plate heights between the forward and bi-directional experiments indicates that the transcolumn contribution to convective dispersion is also important in this column, and can be quantified in a manner similar to the preceding examples involving nonporous particles. As shown in Appendix B, the development given in Section 2 which assumes that all the eluite is present in the interparticle fluid also applies directly to the case where the particles are porous and the eluite becomes adsorbed. The Fourier number, $\tau$, for this column determined using the same method as described above was 0.03 at the flow rate of 0.06 $cm^3$/min, which corresponds to $\nu = 5.4$. From Fig. 6 it can be

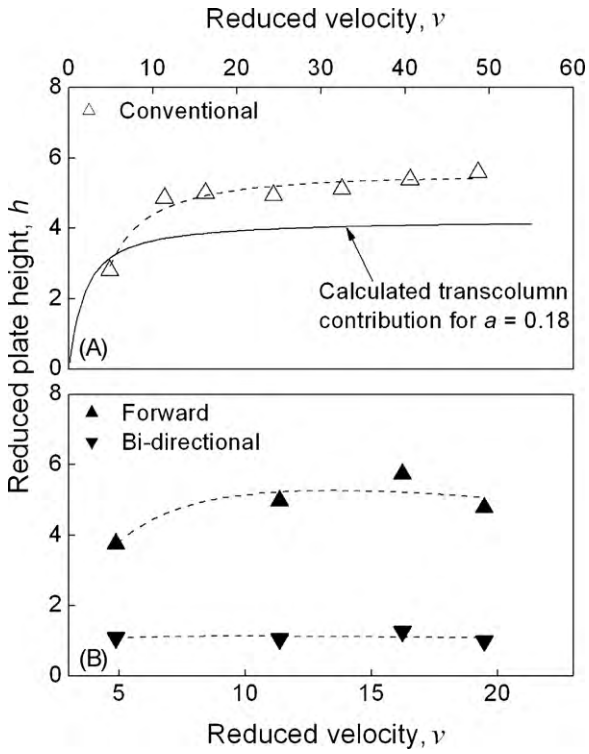


**Fig. 15.** Results from conventional, forward, and bi-directional plate-height experiments using the Omnifit column packed with 85 μm solid glass particles. The feed sample consisted of 2 μl of 1 mg/ml tetrapeptide (Gly-Gly-Tyr-Arg). Mobile Phase: 20 mM Tris, 0.2 M NaCl, pH 9. Dashed curves shown are fits to the empirical Knox equation given by $h = (1/A + 1/(D\nu^n))^{-1} + B/\nu + C\nu$.

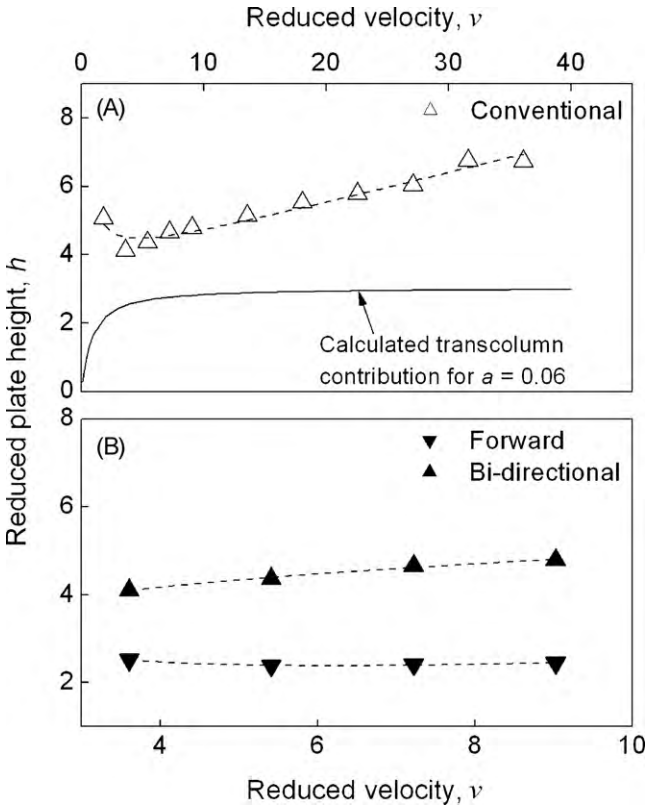


**Fig. 16.** Results from conventional, forward, and bi-directional plate-height experiments using the GE Healthcare Mono Q column. The feed sample consisted of 2 μl of 1 mg/ml tetrapeptide (Gly-Gly-Tyr-Arg). Mobile Phase: 20 mM Tris, 0.2 M NaCl, pH 9. Dashed curves shown are fits to the empirical Knox equation given by $h = (1/A + 1/(D\nu^n))^{-1} + B/\nu + C\nu$.

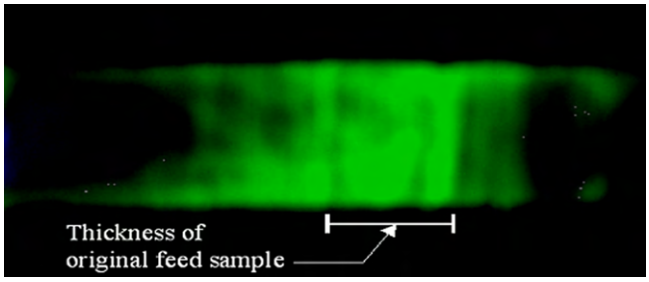


**Fig. 17.** Fluorescence profile of an eluite band in an axial section of a packed column under UV light. The front of the band is on the right side. (For interpretation of the references to color in this figure legend, the reader is referred to the web version of the article.)

seen that this value for the Fourier number corresponds to the border between the intermediate and convection-only regimes. Fig. 16A also shows the theoretically predicted transcolumn plate-height contribution calculated using Eq. (21) and assuming $a = 0.06$, which is the best fitting value of $a$ as determined from the difference in reduced plate heights between the forward and bi-directional experiments in Fig. 16B. The results indicate that in the relatively low-reduced-velocity range considered here, the transcolumn contribution to convective dispersion constitutes approximately one half of the total band broadening, with the remainder of the band broadening evidently resulting from the combination of intracolumn dispersion and intraparticle diffusion.

In order to investigate qualitatively the two-dimensional eluite band shape inside a chromatographic column, the fluorescent dye fluorescene was used under nonbinding conditions to visualize the band shape using an extrusion and sectioning method similar to that described by Kamiński [17]. More specifically, a 10 cm × 0.46 cm I.D. PEEK column was slurry packed with 7-μm solid glass particles as described in Section 3.1. Subsequently, a sample containing fluorescene was injected into the column and allowed to travel 80% of the way from the inlet to the outlet using 20% ethanol as the eluent. The fluid flow was then stopped and the exit end fitting removed. The flow was then restarted and hydraulic pressure was used to extrude the particle bed from the column. Finally, the extruded bed was sectioned axially along its length at the center with a razor blade, and the eluite band photographed under ultraviolet light. Results from this procedure are shown in Fig. 17. Although the detailed two-dimensional band shape of the eluite band in Fig. 17 is somewhat asymmetrical in appearance and partly obscured, evidently because of the relatively simple methods used to obtain that figure, the image obtained nevertheless shows qualitatively the expected "crescent" shape illustrated in Fig. 8.

The Fourier number for the conditions in Fig. 17 was determined using Eq. (17) to be 0.02, and from Fig. 6 it can be seen that this value corresponds to the intermediate transport regime. Note also that value of $\sigma^2_{nr}$ for this case determined by averaging the results from Eqs. (32)–(34) for $\tau = 0.02$ is significantly smaller than the variance contribution that results solely from the original size the feed sample volume used, which was relatively large to ensure that the band could be visualized. More precisely, if the 20-μl volume of the feed sample used is converted into a corresponding length inside the column, the result is $L = 0.34$ cm which, as shown in Fig. 17, corresponds reasonably well to the local thickness of the eluite band at each radial position inside the column. Consequently, the qualitative two-dimensional shape of the eluite band shown in the figure is consistent with the basic assumptions underlying the theory presented in Section 2.

It is useful to compare the results given in this study with those of Kamiński [17] and Moscariello et al. [21] who also compared forward and bi-directional plate-height experiments for particulate columns. In particular, Kamiński found relatively little difference between these two measurements for well-packed preparative-scale HPLC columns. However, Kamiński also observed that the peak shapes observed in his forward-directional experiments were asymmetrical to some extent, and only by ignoring this asymmetry and determining plate heights solely from the measured band width at the band half height was it possible to obtain similar plate heights in the two types of experiments. In contrast, in the present study, peak asymmetry is explicitly accounted for since, as shown in Fig. 4, some degree of asymmetry is expected in the band shape from the transcolumn contribution to convective dispersion for the common case where the intermediate or convection-only regimes apply.

Moscariello et al. [21] also measured forward and bi-directional plate-height experiments for a relatively large process-scale column, and observed a moderate difference in these measurements similar to the results shown in Fig. 12. In addition, by performing these measurements in similarly packed columns of various lengths, these workers concluded that the radial variations in axial fluid velocity responsible for their experimental results was due to fluid flow maldistribution originating in the column header. In contrast, in HPLC columns of the type used in the present study, radial variations in axial fluid velocity are usually thought to result from corresponding radial variations in the interparticle porosity inside the column [27,51]. However, even if the source of the radial variation in axial fluid velocity is the column header (or correspondingly the inlet frit in the case of an HPLC column) or some other localized imperfection inside the column, the theoretical relations and their interpretations described in this study are still expected to be valid, except that the various parameters appearing in these relations, such as the parameter $a$ defined in Eq. (2), become effective averages for the entire column length.

It is also of interest to compare the results obtained in this study with the results of Tallarek et al. [25,28,52] who used pulsed field, gradient nuclear magnetic resonance (PFGNMR) to study dispersion phenomena in chromatographic columns packed with porous particles. As discussed by these workers, the PFGNMR technique is able to detect dispersion phenomena that takes place on a length scale between 10 nm and 100 μm, in which case it is able to measure directly the intracolumn contributions to convective dispersion as defined in Section 2. Accordingly, the difference in the plate heights measured by the conventional plate-height experiments and the PFGNMR experiments by Tallarek et al. as shown in Fig. 18B is a direct measurement of the transcolumn contribution to convective dispersion. The same method described above was used to determine the value of $a$ from the difference in plate heights between the two data sets shown in Fig. 18B, and the theoretically predicted transcolumn plate height for $a = 0.04$, which is the best fitting value of $a$, is shown in Fig. 18A. Note that this value for $a$ corresponds to the value expected for a well-packed column and, similar to the results shown in Fig. 12, the transcolumn contribution to convective dispersion constitutes approximately one half of the total observed band broadening.

The results of this investigation are also relevant to several past studies which have attempted to quantify the magnitudes of the various contributions defined by Giddings for convective dispersion, i.e., the transchannel, short-range interchannel, long-range interchannel, and transcolumn contributions. In particular, in the original work of Giddings [1], the short-range interchannel contribution was predicted to dominate the other contributions except at higher reduced velocities ($\nu > 100$) where this contribution and the transchannel contribution were predicted to become similar in magnitude. However, Giddings also suggested that the magnitude of the transcolumn contribution is difficult to predict *ab initio* and could be the largest contribution in many cases. In a more recent review of past data concerning convective dispersion in chromatographic columns, Knox [5] suggested that the main contribution

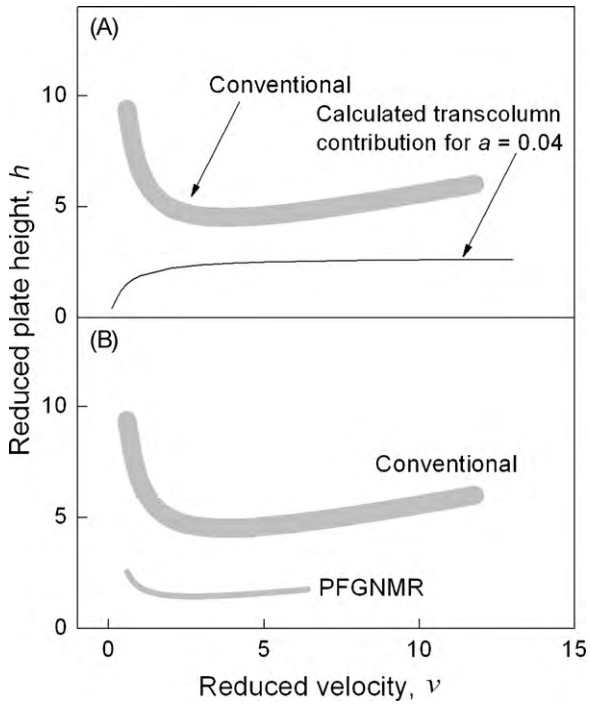


**Fig. 18.** Data obtained by Tallerak et al. [25] for a conventional plate-height experiment and for pulsed field gradient nuclear magnetic resonance (PFGNMR) experiments for the case of 10 cm × 0.44 cm I.D. column packed with 5-μm diameter LiChrosorb RP18 particles. The range of values spanned by the data obtained by Tallerak et al. is represented as a gray band.

to convective dispersion comes from the transcolumn and transchannel contributions. This conclusion was largely based on the observation that experimental plate heights from convective dispersion approach a maximum over a relatively narrow reduced velocity range whose magnitude is consistent with that predicted by Giddings [1] for these two contributions. The results of the present study are consistent with this past work and also extend this past work by confirming that the transcolumn contribution to convective dispersion in many common cases dominates the other contributions.

## 5. Conclusions

This study provides a quantitative foundation for interpreting the difference between conventional and bi-directional plate-height experiments in terms of the various contributions to convective dispersion taking place inside a chromatographic column. It was demonstrated by a combined experimental and theoretical approach that the transcolumn contribution to convective dispersion inside a chromatographic column is generally responsible for the difference between forward and bi-directional plate-height experiments, and that this difference is observable in a wide variety of porous-particle and nonporous-particle columns. More specifically, results obtained in this study indicate that for well-packed columns, including commercially produced columns, approximately one half of the total convective dispersion present is due to the transcolumn contribution, and that this fraction can become even larger under certain conditions, such as for aged or inefficiently packed columns. Furthermore, the variation in axial fluid velocity across the column radius deduced from the amount of convective dispersion measured for this contribution was found to be consistent with past studies where direct measurements have been made of this variation inside chromatographic columns. Consequently, Eq. (21) in Section 2, or its equivalent forms written in terms of $\tau$ or $Pe_r$ given by Eq. (22), can be considered as an improved expression for the $A$-term contribution to the plate-height equation which differs from previous expressions of this type by incorporating an explicit dependence on the ratios $L_c/R_c$ and $R_c/d_p$. In this regard, it can be noted that Broeckhoven and Desmet [53] recently developed an equation similar to Eq. (22) by employing numerical simulations of band broadening in order to fit empirical constants for an assumed functional form of the plate-height relation. The present study therefore provides an experimental verification for this past work as well as an improved theoretical basis for it.

## Nomenclature

*Symbols*

| | |
|---|---|
| $a$, $a'$ | fractional change in velocity across the column radius |
| $c_m$ | eluite concentration in the mobile phase |
| $c_m^*$ | eluite concentration averaged across the column cross-section |
| $c_m^\bullet$ | mixing-cup concentration |
| $D_m$ | molecular diffusion coefficient |
| $D_r$ | radial dispersion coefficient |
| $d_p$ | particle diameter |
| $d_c$ | column diameter |
| $g$ | fractional change in retention factor across the column radius |
| $H$ | plate height |
| $h$ | reduced plate height given by $h = H/d_p$ |
| $k'$ | retention factor |
| $K_{eq}$ | equilibrium distribution ratio |
| $l$ | length of an individual subdomain for a particular convective dispersion contribution |
| $L_c$ | column length |
| $m$ | the mass of feed sample per unit area of column cross-section |
| $n$ | $n$th order velocity profile |
| $N$ | number of plates |
| $n_D$ | the number of movement steps due to diffusive mechanism |
| $n_f$ | the number of movement steps due to flow mechanism |
| $Pe_r$ | radial Peclet number |
| $r$ | radial location in column |
| $R_c$ | column radius |
| $t$ | time or characteristic time |
| $u$ | velocity |
| $\nu$ | reduced velocity given by $\nu = u_{f,ave}d_p/D_m$ |
| $z$ | axial location in column |

*Greek symbols*

| | |
|---|---|
| $\alpha$ | porosity of the particle bed |
| $\gamma$ | tortuosity |
| $\varepsilon$ | intraparticle porosity |
| $\xi$ | dummy integration variable |
| $\lambda$ | dimensionless column aspect ratio defined as $L_c/R_c$ |
| $\tau$ | Fourier number defined as $\tau = D_r t/R_c^2$ |
| $\sigma$ | standard deviation of a Gaussian-shaped eluite band |
| $\phi$ | phase ratio |
| $\psi$ | dimensionless column radius given by $R_c/d_p$ |
| $\omega_\alpha$ | the dimensionless radius of a subdomain given by $r_{domain}/d_p$ |
| $\omega_\beta$ | fractional change in axial fluid velocity across the radius of a subdomain |
| $\omega_\lambda$ | the dimensionless length of a subdomain given by $l_{domain}/d_p$ |
| $\Omega$ | deviation from radial diffusional equilibrium defined as $c_m/c_m^* - 1$ |

*Subscripts*

| | |
|---|---|
| ave | average |
| c | column |
| CE | close-to-equilibrium |
| cl | centerline |
| CO | convection only |
| domain | property of a subdomain |
| e | effective average as defined in Appendix B |
| f | interparticle fluid |
| fm | first moment |
| max | maximum |
| min | minimum |
| nr | not affected by flow direction |
| *t* | time |
| total | total amount |
| WS | Wang and Stewart |
| *z* | axial distance |

**Acknowledgements**

Support from grants 0442072 and 0854151 from the National Science Foundation is greatly appreciated. We also thank Delphilia Burton (GlaxoSmithKline) and Archana Raamanathan (University of Texas, Austin) for their useful preliminary work related to this study and for many helpful comments.

## Appendix A. Relation between Eq. (4) and the Giddings dispersion theory

If the fractional change in the axial fluid velocity in the domain of interest (i.e., the transcolumn, transchannel, short-range interchannel, or long-range interchannel domain) is defined as $\omega_\beta = a u_{f,cl}/u_{f,ave} = \Delta u/u_{f,ave}$, then the result given by Eq. (4) for the plate height in the close-to-equilibrium regime for $n = 2$ can be generalized to any domain and rewritten as

$$H_{CE} = \frac{\omega_\beta^2 \omega_\alpha^2 u_{f,ave} d_p^2}{96 D_r} \tag{A.1}$$

Eq. (A.1) can be compared with the following result given by Giddings [1] for this same case, termed the "diffusive mechanism" plate height, which is based on the qualitative application of random walk theory to a velocity profile specified by the parameter $\omega_\beta$ (see Eq. (2.10-6) of Ref. [1]):

$$H_D = \frac{\omega_\beta^2 \omega_\alpha^2 u_{f,ave} d_p^2}{2 D_m} \tag{A.2}$$

The large disparity in the numerical factors in the denominators of Eqs. (A.1) and (A.2), and the fact that Eq. (A.1) employs the radial dispersion coefficient while Eq. (A.2) employs the molecular diffusion coefficient, is notable and evidently results from the qualitative approach used to develop the latter equation. It can also be seen in this regard that Eq. (A.1), but with $D_m$ substituted for $D_r$, is equivalent to the result for $n = 2$ given by the generalized nonequilibrium theory of Giddings (see Eq. (4.5-22) of Ref. [1]) and that the difference between Eqs. (A.1) and (A.2) has been previously noted by Giddings (see Section 2.12 of Ref. [1]) and by Tijissen (see Section II.E.4e of Ref. [40]).

In order to develop a complete theory of dispersion for each domain of interest, Giddings [1] combined the diffusive result given by Eq. (A.2) with a "flow mechanism" result based on the assumption that an eluite makes a random distance step in the $z$ direction of length $l_{domain}\Delta u/u_{f,ave}$ with respect to the average position of the band each time the eluite travels between the individual subdomains for each type of dispersion contribution. The final result obtained by Giddings on this basis can be written as:

$$h = \frac{1}{1/(\omega_\beta^2 \omega_\lambda) + 2/(\omega_\beta^2 \omega_\alpha^2 \nu)} \tag{A.3}$$

Eqs. (A.1) and (A.3) can be compared for the particular case of the transcolumn contribution to dispersion by incorporating the proposed optimal correlation for radial dispersion given in Fig. 3 in the former equation, and by using the approximation $\omega_\lambda = 20\omega_\alpha^2$ suggest by Gidddings [1] in the latter equation. These substitutions yield the following two results:

$$h = \frac{20\omega_\beta^2 \omega_\alpha^2}{1 + 40/\nu} \tag{A.4}$$

and

$$h = \frac{0.21\omega_\beta^2 \omega_\alpha^2}{1 + 15.5/\nu} \tag{A.5}$$

where Eqs. (A.4) and (A.5) apply to the Giddings random walk theory as just described and the theory developed in this study, respectively. A comparison of Eqs. (A.4) and (A.5) indicates that the most significant discrepancy in the two results is that the maximum values of $h$ at large values of $\nu$ differ by two orders of magnitude, so that the two results yield very different values of $\omega_\beta^2$ for a given value of $\omega_\alpha^2$ when fitting the same experimental data.

## Appendix B. Extension of theory to the case where $\varepsilon > 0$ and $k' > 0$

The development in Section 2 applies specifically to the case of a nonporous particle and an unadsorbed eluite where $k' = 0$, where $k' = \phi K_{eq}$. Note that $K_{eq}$ is the equilibrium distribution ratio and $\phi$ is the phase ratio given by $(1-\alpha)(1-\varepsilon)/(\alpha + (1-\alpha)\varepsilon)$ where $\varepsilon$ is the intraparticle porosity and $\alpha$ is the interparticle porosity. The case for a porous particle where $\varepsilon > 0$ and $k' > 0$ can be addressed by first observing that the relation between the radial Peclet number and the reduced velocity given in Fig. 3 is independent of the values of $k'$ and $\varepsilon$ provided that the eluite within the exterior surface of a porous particle has no net radial or axial motion inside the column. This follows from the fact that when $k' > 0$ and $\varepsilon > 0$, $Pe_r$ is evaluated as $u_e d_p/D_{r,e}$, where the subscript "e" denotes the effective mole average value of a quantity. If the portion of the eluite within a particle has no net motion, then

$$u_e = \frac{u_f}{(1 + (1-\alpha)\varepsilon/\alpha)(1 + k')} \tag{B.1}$$

and

$$D_{r,e} = \frac{D_r}{(1 + (1-\alpha)\varepsilon/\alpha)(1 + k')} \tag{B.2}$$

so that $u_e d_p/D_{r,e} = u_f d_p/D_r = Pe_r$.

The relations developed in Section 2 for the various transport regimes can be extended *mutatis mutandis* to the case where $\varepsilon > 0$ and $k' > 0$ by assuming that the eluite portion outside the particles moves at the axial velocity $u_f$ and is subject to a radial dispersion coefficient equal to $D_r$, while the eluite portion inside the particles is again assumed to be motionless, and then replacing the fluid velocity used in the relations in that section with the mean velocity of the eluite. Consequently, $u_f$ in Section 2 can be replaced by the average eluite species velocity $u_e$ given above, and the parameter $a$ employed in Section 2, which is re-named $a'$ here, can be defined as $u_e = u_{e,cl}(1 - a' r^n/R^n)$. If, in addition, the radial variation in $u_e$ is attributed to simultaneous radial variations in $u_f$ and $k'$, and if $n$th order functions are assumed for these variations, it follows from

Eq. (B.1) that

$$u_e = \frac{u_{f,cl}(1 - ar^n/R_c^n)}{(1 + (1-\alpha)\varepsilon/\alpha)(1 + k'_{cl}(1 - gr^n/R_c^n))} \quad (B.3)$$

If the right side of Eq. (B.3) is expanded in a Taylor series in $r$ assuming $k' \gg 1$, and if the terms in this series above the second order term are ignored, the result can be written as

$$u_e \approx \left[\frac{u_{f,cl}}{(1 + (1-\alpha)\varepsilon/\alpha)(1 + k'_{cl})}\right](1 - (a-g)r^n/R_c^n) \quad (B.4)$$

where the quantity in square brackets in Eq. (B.4) is $u_{e,cl}$. It can therefore be seen that $a' \approx a - g$, which indicates that when $k' \gg 1$ fractional changes in $u_f$ across the column radius have the same effect on the plate height as an equivalent fractional change in $k'$, and that the two effects are additive. A similar conclusion was arrived at by Giddings [54] in his development of the general form of Eq. (3) given in Section 2.1.1 (see the discussion of Eq. (30) in Ref. [54]).

## References


[1] J.C. Giddings, Dynamics of Chromatography, Part I. Principles and Theory, Marcel Dekker, New York, 1965.
[2] J.J. van Deemter, F.J. Zuiderweg, A. Klinkenberg, Chem. Eng. Sci. 5 (1956) 271.
[3] J.H. Knox, H.P. Scott, J. Chromatogr. 282 (1983) 297.
[4] J.H. Knox, J. Chromatogr. A 831 (1999) 3.
[5] J.H. Knox, J. Chromatogr. A 960 (2002) 7.
[6] A.B. Littlewood, in: A. Goldup (Ed.), Gas Chromatography 1964, Institute of Petroleum, London, 1965, p. 77.
[7] M.A. Teeters, I. Quiñones-García, J. Chromatogr. A 1069 (2005) 53.
[8] D.D. Frey, E. Schweinheim, Cs. Horváth, Biotechnol. Prog. 9 (1993) 273.
[9] N. Ishizuka, H. Kobayashi, H. Minakuchi, K. Nakanishi, K. Hirao, K. Hosoya, T. Ikegami, N. Tanaka, J. Chromatogr. A 960 (2002) 85.
[10] F. Gritti, A. Cavazzini, N. Marchetti, G. Guiochon, J. Chromatogr. A 1157 (2007) 289.
[11] J.J. Kirkland, F.A. Truszkowski, C.H. Dilks Jr., G.S. Engel, J. Chromatogr. A 890 (2000) 3.
[12] P.A. Bristow, J.H. Knox, Chromatographia 10 (1977) 279.
[13] A.S. Rathore, R.M. Kennedy, J.K. O'Donnell, L. Bemberis, O. Kaltenbrunner, Elements of Biopharmaceutical Production Series, Advanstar Communications Inc., New York, 2007, p. 26.
[14] Z.K. López, A. Tejeda, J. Chromatogr. A 791 (1997) 99.
[15] C.T. Wehr, J. Chromatogr. 418 (1987) 27.
[16] C.H. Eon, J. Chromatogr. 149 (1978) 29.
[17] M. Kamiński, J. Chromatogr. 589 (1992) 61.
[18] D.K. Roper, E.N. Lightfoot, J. Chromatogr. A 702 (1995) 69.
[19] J. Moscariello, G. Purdom, J. Coffman, T.W. Root, E.N. Lightfoot, J. Chromatogr. A 908 (2001) 131.
[20] M.A. Teeters, S.E. Conrardy, B.L. Thomas, T.W. Root, E.N. Lightfoot, J. Chromatogr. A 989 (2003) 165.
[21] J. Moscariello, E. Lightfoot, A. Rathore, Elements of Biopharmaceutical Production Series, Advanstar Communications Inc., New York, 2007, p. 41.
[22] K. Miyabe, G. Guiochon, J. Chromatogr. A 830 (1999) 29.
[23] K. Miyabe, G. Guiochon, J. Chromaogr. A 857 (1999) 69.
[24] T. Farkas, G. Guiochon, Anal. Chem. 69 (1997) 4592.
[25] U. Tallarek, K. Albert, E. Bayer, G. Guiochon, AIChE J. 42 (1996) 3041.
[26] J.E. Baur, E.W. Kristensen, R.M. Wightman, Anal. Chem. 60 (1988) 2334.
[27] T. Farkas, J.Q. Chambers, G. Guiochon, J. Chromatogr. A 679 (1994) 231.
[28] U. Tallarek, E. Bayer, G. Guiochon, J. Am. Chem. Soc. 120 (1998) 1494.
[29] D.D. Frey, X. Kang, Curr. Opin. Biotechnol. 16 (2005) 552.
[30] A.M. Athalye, S.J. Gibbs, E.N. Lightfoot, J. Chromatogr. 589 (1992) 71.
[31] G.I. Taylor, Proc. Roy. Soc. A 219 (1953) 186.
[32] G.I. Taylor, Proc. Roy. Soc. A 225 (1954) 473.
[33] R. Aris, Proc. Roy. Soc. A 235 (1956) 67.
[34] K.B. Bischoff, O. Levenspiel, Chem. Eng. Sci. 17 (1962) 257.
[35] R.A. Shalliker, B.S. Broyles, G. Guiochon, J. Chromatogr. A 888 (2000) 1.
[36] G. Guiochon, T. Farkas, H. Guan-Sajonz, J. Koh, M. Sarker, B.J. Stanley, T. Yun, J. Chromatogr. A 762 (1997) 83.
[37] J.H. Knox, J.F. Parcher, Anal. Chem. 41 (1969) 1599.
[38] J.H. Knox, G.R. Laird, P.A. Raven, J. Chromatogr. 122 (1976) 129.
[39] T.K. Perkins, O.C. Johnston, Soc. Pet. Eng. J. 3 (1963) 70.
[40] R. Tijssen, in: E. Katz, R. Eksteen, P. Schoenmakers, N. Miller (Eds.), Handbook of HPLC, Marcel Dekker, Inc., New York, 1998, p. 55.
[41] D.J. Gunn, Chem. Eng. Sci. 42 (1987) 363.
[42] J.S. Vrentas, C.M. Vrentas, AIChE J. 34 (1988) 1423.
[43] T. Yun, G. Guiochon, J. Chromatogr. A 672 (1994) 1.
[44] H. Guo, Masters Thesis, University of Maryland Baltimore County, Baltimore, MD, 2008, http://proquest.umi.com/pqdweb?index=4&did=1666876241&SrchMode=1&sid=6&Fmt=6&VInst=PROD&VType=PQD&RQT=309&VName=PQD&TS=1246640251&clientId=11430.
[45] T. Fornstedt, G. Zhong, G. Guiochon, J. Chromatogr. A 742 (1996) 55.
[46] J.C. Wang, W.E. Stewart, AIChE J. 29 (1983) 493.
[47] J.A. Abia, K.S. Mriziq, G. Guiochon, J. Chromatogr. A 1216 (2009) 3185.
[48] J.P. Foley, J.G. Dorsey, Anal. Chem. 55 (1983) 730.
[49] M.M. Fallas, M.R. Hadley, D.V. McCalley, J. Chromatogr. A 1216 (2009) 3961.
[50] F. Lottes, W. Arlt, M. Minceva, E.H. Stenby, J. Chromatogr. A 1216 (2009) 5687.
[51] T. Farkas, M.J. Sepaniak, G. Guiochon, J. Chromatogr. A 740 (1996) 169.
[52] U. Tallarek, D.V. Dusschoten, H.V. As, E. Bayer, G. Guiochon, J. Phys. Chem. B 102 (1998) 3486.
[53] K. Broeckhoven, G. Desmet, J. Chromtogr. A 1216 (2009) 1325.
[54] J.C. Giddings, J. Gas Chromatogr. 1 (1963) 38.